Master's Dissertation
TVVR 08/5010

Hydrodynamic modelling and estimation of exchange rates for Bardawil Lagoon, Egypt.

An investigation of governing forces and physical processes using numerical models.

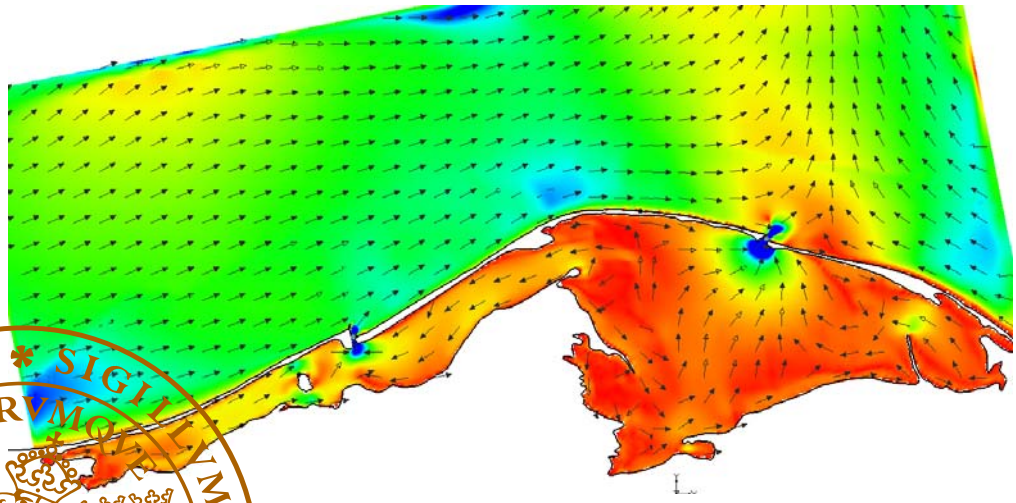

Jonas Linnersund
Erik Mårtensson

Division of Water Resources Engineering
Department of Building and Environmental Technology
Lund Institute of Technology
Lund University

Division of Water Resources Engineering
ISRN LUTVDG/TVVR-08/5010+88p
ISSN-1101-9824

Hydrodynamic modelling and estimation of exchange rates for Bardawil Lagoon, Egypt.

An investigation of governing forces and physical processes using numerical models.

Jonas Linnersund
Erik Mårtensson

Supervisor
Magnus Larson[1]

Division of Water Resources Engineering
Department of Building and Environmental Technology
Lund Institute of Technology
Lund University

November 2008

Printed in Sweden

[1] Professor, Division of Water Resources Engineering, Lund Institute of Technology

LUNDS TEKNISKA HÖGSKOLA
Lunds universitet

Lund University
Faculty of Engineering, LTH
Departments of Earth and Water Engineering

This study has been carried out within the framework of the Minor Field Studies (MFS) Scholarship Programme, which is funded by the Swedish International Development Cooperation Agency, Sida.

The MFS Scholarship Programme offers Swedish university students an opportunity to carry out two months' field work in a developing country resulting in a graduation thesis work, a Master's dissertation or a similar in-depth study. These studies are primarily conducted within subject areas that are important from an international development perspective and in a country supported by Swedish international development assistance.

The main purpose of the MFS Programme is to enhance Swedish university students' knowledge and understanding of developing countries and their problems. An MFS should provide the student with initial experience of conditions in such a country. A further purpose is to widen the human resource base for recruitment into international co-operation. Further information can be reached at the following internet address: http://www.tg.lth.se , click at "MFS-stipendier".

The responsibility for the accuracy of the information presented in this MFS report rests entirely with the authors and their supervisors.

Gerhard Barmen
Local MFS Programme Officer

Postadress Box 118, 221 00 Lund *Besöksadress* John Ericssons väg 1*Telefon dir* 046-222 9657, *växel* 046-222 00 00 *Telefax* 046-2229127
E-post Gerhard.Barmen@tg.lth.se

Abstract

Bardawil Lagoon, a natural lagoon located on the northern coast of the Sinai Peninsula, Egypt, there are three inlets of which two are man-made connecting the lagoon with the Mediterranean Sea. The inlets are subjected to changes in morphology, due to sediment transport, over time and this may lead to degrees of closure of either inlet. The sediment transport is governed by longshore currents and the sediments originate from the eroding Nile delta. Inlet closure adversely affects the lagoon water quality which will have a detrimental effect on the ecosystem.

In this dissertation the dominant coastal processes governing the water exchange between the lagoon and the Mediterranean are studied. Finite element conceptual computer models are applied to simulate and investigate the hydrodynamics of the inlets and the lagoon itself. Two types of models are applied within the Surface Modelling System (SMS) software; ADCIRC, a regional tidal model and CMS-Flow, a local circulation model. In order to estimate the exchange rate of the lagoon two methods are utilized; based on net intertidal volume and cross sectional flow through the inlets. The methods show a high degree of correlation. The renewal time was estimated to 9.0 days, which is equivalent to a daily replaced volume of $53 \cdot 10^6$ m^3. Tidal forcing governs the water exchange while wind is responsible for the internal circulation.

Keywords: **ADCIRC, Bardawil Lagoon, CMS-Flow, finite element, internal circulation, net intertidal volume, renewal time, salt balance, sediment transport, tide, water balance, wind**

Preface

This Master's Dissertation report is the result of a combined field study and computer modelling of the hydrodynamics of Bardawil Lagoon, Egypt. The project was carried out in order to gain a further understanding of the coastal processes affecting the inlets and how manage them to preserve the clean environment and lagoon water quality. The project was a joint venture between Lund University, Division of Water Resources Engineering and Suez Canal University.

Despite persistent attempts to obtain permission to visit the lagoon and conduct field measurements we failed to receive a permit. However, thanks to Coastal Research Institute in Alexandria, we managed to acquire necessary measurements from earlier studies.

Acknowledgements

We would like to express our gratitude to SIDA, Ångpanneföreningen's Foundation for Research and Development and Swedish Association of Graduate Engineers for financial support of our Master's Dissertation which includes a two month field study in Egypt. Dr. Yasser Hamed at Suez Canal University, Port Said, for practical help in Port Said and the endless efforts in trying to obtain permission to visit the site. Prof. Ibrahim El-Shinnawy and Dr. Madhat Mohamed at Coastal Research Institute (CoRI) in Alexandria, for their hospitality and most importantly providing invaluable field data. Prof. Hans Hanson at the Division of Water Resources Engineering, Lund, and Dr. Ahmed Ahmed at Hydraulics Research Institute, Cairo, for guidance on theory and computer modelling. AB Teknoplan in Stockholm for digitizing field data and maps obtained in Egypt. Special thanks to Prof. Omran Frihy for his continuous interest in our work and its progress and providing us with interesting ideas throughout our stay in Egypt.

During the course of constructing the 2D-finite element models within the Surface Modelling System software, several difficulties arose and without the help and technical support from both Adele Buttolph at Coastal Analysis, LLC Oregon, and Mitchell Brown at US Army Corps of Engineers the modelling would have been impossible. Also special thanks to US Army Corps of Engineers for providing us with licence to the software suite and the models.

Finally our deepest appreciation to our supervisor Prof. Magnus Larson at the Division of Water Resources Engineering, Lund, for extraordinary expertise and assistance throughout the dissertation.

Table of contents

1 Introduction

1.1 Background

Coastal lagoons are defined as water bodies separated from the sea by a land barrier, which through one or many inlets is connected with the sea. Coastal lagoons are often located in areas with a low topographical level and small or moderate tidal changes (Oertel, 2005). It is estimated that lagoons constitute approximately 13% of the total world coastline and they exist in many places, *e.g.*, the southern Baltic Sea, Black Sea, Caspian Sea, Mediterranean Sea, and the Gulf of Mexico (Kjerfve, et al., 1996).

Sediment transport due to coastal waves and currents is a naturally occurring phenomenon, which is typically driven by offshore waves that generate longshore sediment transport as they strike the coastline at an angle. Gradients in the longshore sediment transport cause erosion and accretion resulting in different types of problems to be addressed by coastal engineers and managers. The complex flow, sediment transport, and morphological evolution at coastal inlets often induce patterns of accumulation in and around the opening that causes a wide range of engineering problems.

At Bardawil Lagoon, a natural lagoon located on the northern coast of the Sinai Peninsula, Egypt, three inlets, of which two are man-made, connect the lagoon with the Mediterranean Sea. The inlets are subjected to changes in the morphology over time, including sediment infilling of the inlet channels. Persistent coastal currents and waves shape the morphology, as well as short-term events such as storms. Because the hydrodynamics, sediment transport, and inlet morphological change are connected, it is important to understand the interaction between these processes in order to minimize channel dredging and to promote the water exchange between the lagoon and the sea (US Army Corps of Engineers, 2007). Dredging is an expensive and complex procedure, hence it is favourable to investigate solutions that can increase sediment bypassing and stabilise the inlets. The siltation at the inlets leads to reduced water exchange between the lagoon and the sea resulting in poorer circulation in the lagoon and degradation of the water quality. This greatly affects fish growth and reproduction in the lagoon, which the fishing industry in the area depends on. It is therefore desirable to construct a predictive model that can assess and estimate the exchange rate with the Mediterranean and the effects of changes in inlet morphology.

In order to manage the lagoon and its inlets, the physical processes that govern the renewal time must be understood. The main concept of the present report is the renewal time, which depends on the amount of water that is able to pass through the narrow inlets during each tidal cycle. To gain an improved understanding of the exchange, significant processes determining this exchange, such as tidal action and wind, have been thoroughly examined in this study.

1.2 Objectives

The main objectives of this report are:

- Develop a conceptual model of the water exchange in the lagoon based on detailed numerical modelling of the water circulation.
- Identify the main physical processes that govern the water exchange and circulation in Bardawil Lagoon.
- Estimate the exchange rate between the lagoon and the Mediterranean Sea, including the renewal time of the lagoon.
- Investigate the effects on the water quality due to reduced water flow through the inlets because of sedimentation.

1.3 Procedure

Published material, such as journal articles, conference papers, books, and reports, as well as unpublished material, was studied in order to gain a comprehensive understanding of the coastal processes that govern the water exchange and inlet morphology of coastal lagoons in general and of Bardawil Lagoon in particular. The review of existing material also resulted in much needed data for the analysis and modelling. Prior to this investigation, the exchange rate of Bardawil Lagoon has never been determined; hence comparative data for validation are non-existent. The literature available that deals with this topic derives from other sites.

A two-month visit was made to Egypt and a site visit to Bardawil Lagoon was planned during this visit. The main purpose of the site visit was to collect data at the lagoon, including bathymetry, currents, salinity, sand deposition, and erosion. However, it was deemed unsafe to perform such a visit because of the current political situation between Egypt and Israel/Palestine, and the fear of terrorist attacks. Thus, the Egyptian authorities did not grant us permission to visit the lagoon to conduct any field measurements. Since we were unable to conduct any measurements, we had to change our approach to obtain data for the investigation. Rather than collecting data our self, we focused on working with previously established contacts between Lund University and other institutions in Egypt, mainly Coastal Research Institute in Alexandria. These institutions were able to provide us with various data that allowed for a successful completion of the study.

Evaluation of the available data and associated simulations were performed using a computer model suite known as SMS (Surface Modelling System). The package contains several different purpose-specific models, such as CMS-Flow and ADCIRC. These two models were applied in this project and they are presented in more detail later in the report. Design and construction of the models are broken up into functional element layers, *e.g.*, maps and coastlines (map module), bathymetric data (scatter module), interpolated data sets, and finite element grids (grid module). The grid is sub-divided into several elements which may be lumped into larger segments. The advantage of working with layers is that the user can freely modify one component without affecting the others. Layers can be divided into two categories;

raw data layers and derived calculated layer sets. Each model is governed by a set of equations and the parameterizations of these equations are controlled via the “model control” as is the timing of each model. Timing includes variables such as model time step, simulation run time, and output control (results).

2 Area description

2.1 Physical characteristics

The Mediterranean coast of the Sinai Peninsula stretches from the Suez Canal in the west to the Israeli/Palestinian border in the east. Bardawil Lagoon, also referred to as Bardawil Lake in some studies, is one of the major features of the coastline and is located at latitude 31˚03'-31˚15'N and longitude 32˚40'-33˚32'E (Figure 1). The lagoon is of tectonic origin compared to the other Mediterranean Egyptian lagoons, for example, Idku, Burullus, and Manzala, which are of deltaic origin (the Nile River Delta) (El-Bana, et al., 2002). Bardawil Lagoon is the largest and least polluted lagoon in Egypt (Fanos, et al., 1994) (ramsar.org, 1991).

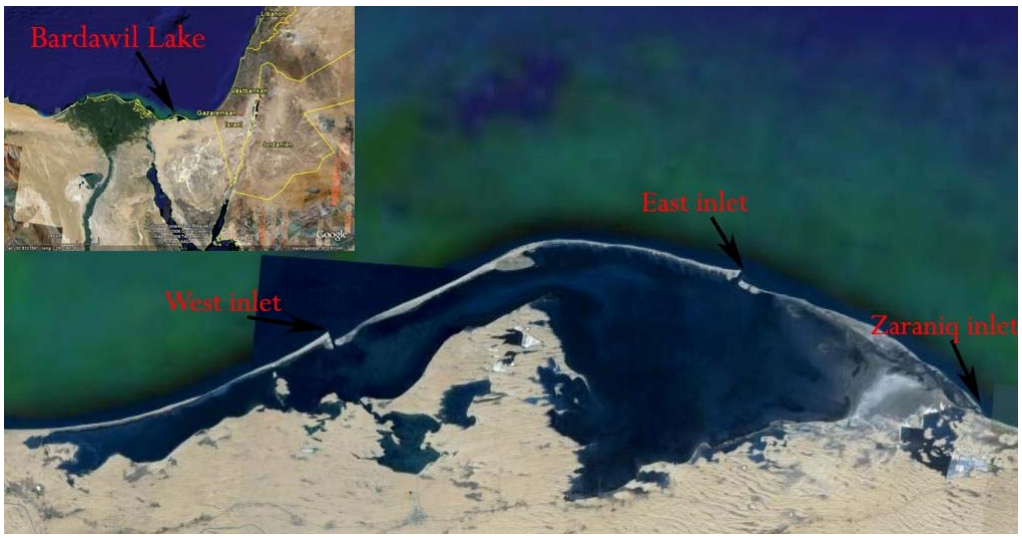

Figure 1: Map of the study area Bardawil Lagoon, Egypt (Google, 2007).

Bardawil Lagoon stretches a distance of 80 km, has a width of 18 km, and is separated from the Mediterranean Sea by a curving sand barrier with a width of 300-2000 m (El-Bana, et al., 2002) (Levy, 1974). The lagoon was, in its natural state, a dry salt pan which from time to time was filled with water when the sand barrier was breached by storm waves. When all its various branches are filled with water it covers an area of approximately 600 km^2 (Inman, et al., 1970). The water covered area varies during the year with separate ponds and lakes created during the hot summer months. Bardawil Lagoon is a shallow lagoon with a maximum depth of 2.5-3 m, found in the western arm, and an average depth of 1.5-1.75 m (Figure 2). There are a few islands and saline flats known as sabkhahs, particularly in the east (El-Bana, et al., 2002) (Inman, et al., 1970). The lagoon is permanently hyper saline with a water salinity of 45‰ near the inlets and 65‰ in the fringes compared to the salinity of 39‰ in the Mediterranean. Salinity levels exceeding 90‰ have been measured at times when one of the inlets was clogged by sediment (Fanos, et al., 1994).

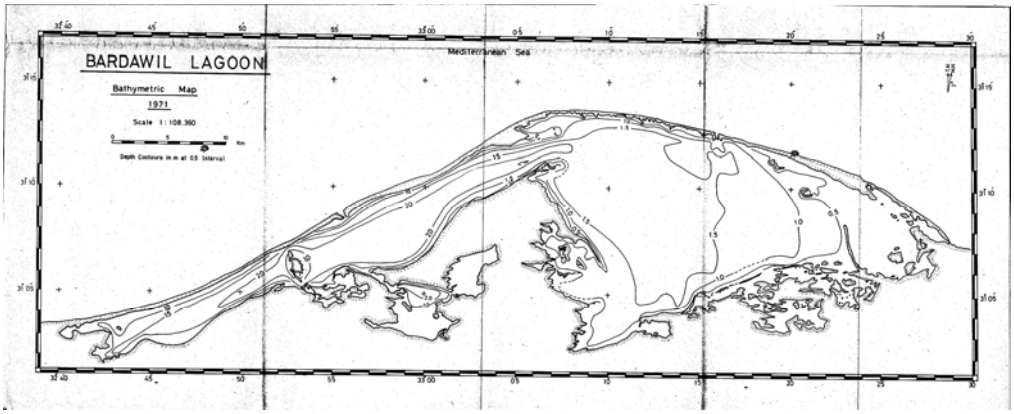

Figure 2: Map of Bardawil Lagoon with depth contours (Coastal Research Institute, 1971-1999).

In the beginning of the 20th century Bardawil Lagoon was artificially opened so it could be used for fishing purposes. The lagoon had an opening and closing cycle of approximately three years: 6 months to open the inlets by digging and thereby connecting the lagoon with the sea, 24 months of fishing before the inlets were closed by littoral drift, and finally 6 months before the lagoon became dry due to evaporation. In 1927 dredging began and at least 5 different entrances were dug until 1953 when two large inlets with concrete jetties were established. Maintenance of both inlets was performed by continuous dredging and extension of the jetties until 1967 when it was concluded that the efforts were insufficient to keep the entrance of the eastern inlet open (Inman, et al., 1970). Dredging was re-established three years later with more efficient equipment and it was re-opened in 1972. Since this time the inlets have been kept open but with constant changes in morphology (Klein, 1986). In order to further reduce the need for dredging and stabilize the inlets the western and eastern jetties of both inlets were moved and rebuilt with exception for the western jetty of the west inlet which was kept intact. These protective works were carried out and finalized around 1995 (Dr. Madhat, 2008).

Today there are three inlets connecting the lagoon with the Mediterranean Sea: the western inlet, the eastern inlet, and the natural inlet, Zaraniq, which has never been dredged and therefore is closed from time to time (Figure 1 and Figure 3) (El-Bana, et al., 2002).

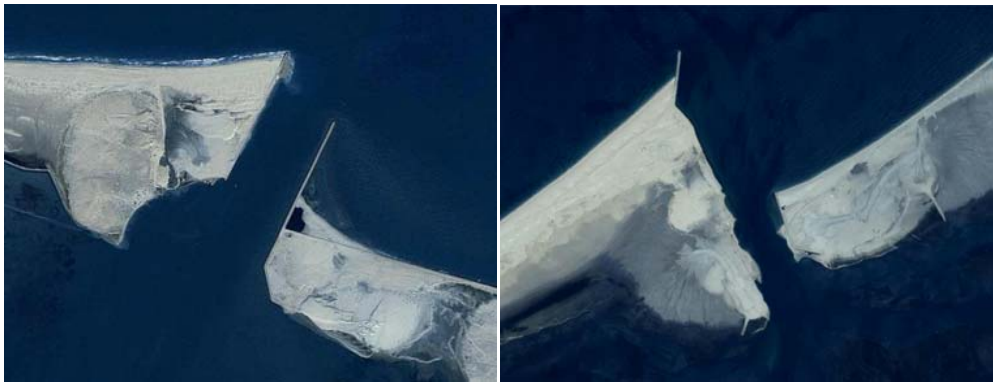

Figure 3: Pictures of the west and east inlet (Google, 2007).

2.2 Climate

Bardawil Lagoon has an arid Mediterranean climate with a mean annual rainfall of less than 100 mm. There are no tributaries to the lagoon so the only freshwater reaching Bardawil Lagoon is the scarce winter rain, from October to May (Figure 4) (Levy, 1974) (Coastal Research Institute, 2008). The average monthly temperatures vary between 14°C in January to 28°C in July (Figure 5). The evaporation rate depends on the temperature and therefore has a seasonal variation (Figure 6). Other evaporation estimations vary between 2000 mm/year (Levy, 1977) and 3650 mm/year (Inman, et al., 1970). The temperature of the Mediterranean Sea varies over the year between 15.4 and 22.7˚C (Fanos, et al., 1994) while the lagoon water can reach temperatures of 32˚C in the summer (El-Bana, et al., 2002).

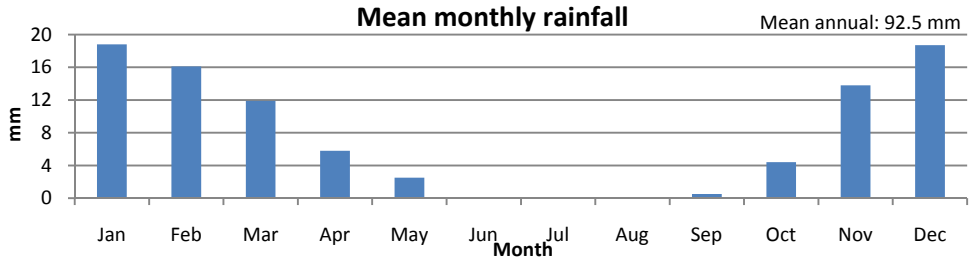

Figure 4: Mean monthly rainfall at Bardawil Lagoon (Coastal Research Institute, 2008).

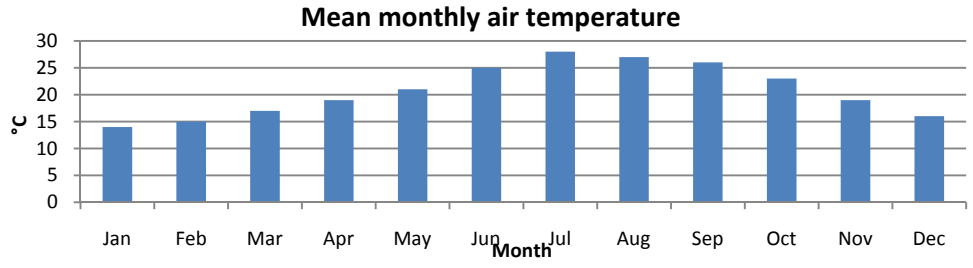

Figure 5: Mean monthly air temperature at Bardawil Lagoon (Coastal Research Institute, 2008).

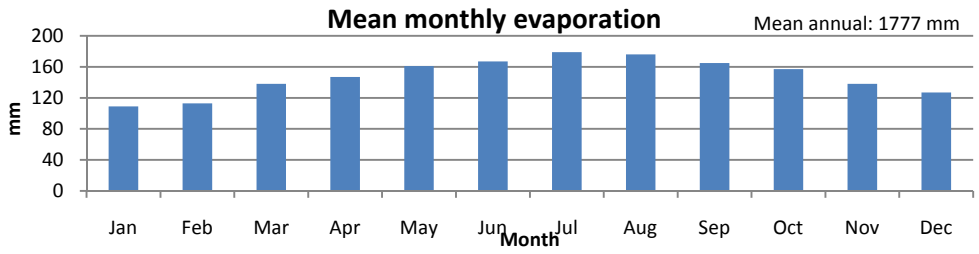

Figure 6: Mean monthly evaporation at Bardawil Lagoon (Coastal Research Institute, 2008).

2.3 Human activities

North Sinai is a low-density populated area and the few ten thousands of inhabitants that populate the area are scattered out in small villages (Inman, et al., 1970). Approximately 15% of the people living in the region get their income from activities related to the fishing in the lagoon (ramsar.org, 1991). Each year the Bardawil Lagoon yields 1500-2000 tons of fish, which is both consumed by the local inhabitants and exported abroad (Fanos, et al., 1994). The lagoon is an important spawning area for fish and commercially important fish species in the lagoon are the Gilthead Seabream *(Sparus aurata),* Striped Mullet *(Mugil cephalus),* European Seabass *(Dicentrarchus labrax),* Shade-fish *(Argyrosomus regium),* Common Sole *(Solea solea),* and the White Grouper (*Epinephelus aeneus).* Fishing is regulated and the number of fishing boats is limited as well as the horsepower strength of their engines (ramsar.org, 1991). Fish growth and reproduction are dependent on a good circulation and renewal of lagoon water (Fanos, et al., 1994). Besides being an important spawning area for many fish species the lagoon area is a popular site for many wintering and staging water birds. Each year more than 500,000 birds use the lagoon as a refuelling stop when migrating (ramsar.org, 1991).

In the very shallow, eastern parts of the lagoon an extensive salt production system has been established with evaporation ponds, salt washing, and drying and storage facilities (ramsar.org, 1991). Other industries are mainly concerned with palm and olive oil production and have little impact on Bardawil Lagoon (Coastal Research Institute, 2008).

The Egyptian government is planning to divert Nile water under the Suez channel and to irrigate the area south of Bardawil Lagoon. It is estimated that this will lead to a population increase of 200,000-300,000 people in the north Sinai area (ramsar.org, 1991). At present the canal is under construction but once finished the agricultural activity and thereby the discharge of agricultural drainage water to Bardawil Lagoon will increase and adversely affect the water quality (Coastal Research Institute, 2008).

3 Coastal Processes at Bardawil Lagoon

3.1 Wind climate

Wind is an important factor in maintaining a good circulation of the water within Bardawil Lagoon as well as exchange with the sea (Miller, et al., 1990). Also, the wind generates waves that are responsible for the longshore currents transporting sediment to the lagoon inlets and thereby decreasing the exchange rate with the Mediterranean Sea.

Available wind data closest to the study area are measured at Port Said, which is situated approximately 60 km west of Bardawil Lagoon. It is assumed that these data are representative for the lagoon area. Two data series of wind measurements were available: one is stretching from July 1999 to June 2000 and one is covering the whole year of 2005. There are two data gaps in the measurements from the 1999-2000 data series. The first gap starts 28 July and ends 3 August 1999, while the second gap starts 30 November 1999 and ends 4 January, 2000. The data series from 2005 are complete except for about 50 hours of measurements. Both data series contain hourly measurements of the mean wind speed and direction. However, the wind speed is rounded off to the closest integer for the data from 2005, whereas there are two decimals in the other data series. Also, the direction is given with two significant digits for 2005, wheras it is given with three significant digits for the earlier data series. The most frequent wind directions are between NW and N, with 44% of the winds approaching from these directions during 2005 and 31% during July 1999 to June 2000 (Figure 7). The average wind speeds for the mean hourly measurements are 3.69 m/s and 4.92 m/s respectively, with the highest value representing 2005. The difference in average wind speed between the years might be explained by the differences in the data series presented above. Also, all measurements from December 1999 are missing.

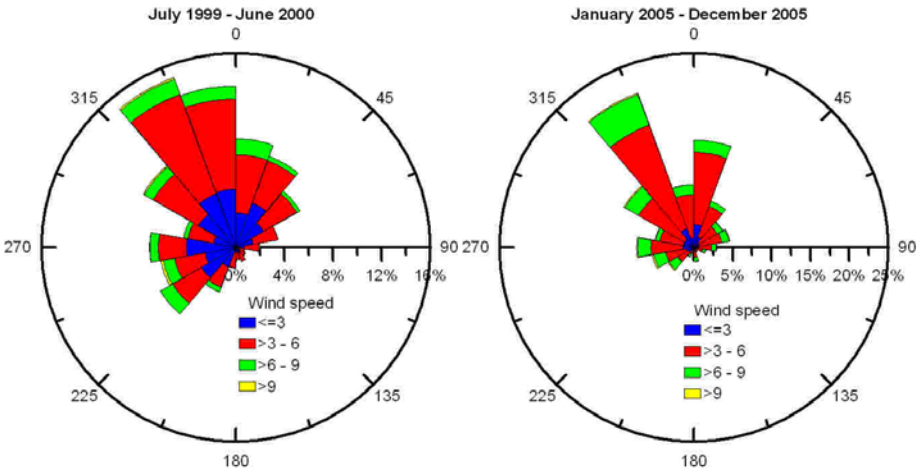

Figure 7. Wind roses (m/s) from 1999-07-01 to 2000-06-30, and 2005-01-01 to 2005-12-31.

The prevailing wind direction changes over the year, depending on the season (Figure 8). During January and February, strong winds are approaching from SW to W, with maximum mean hour wind speeds exceeding 13 m/s. The wind direction during spring, from March to April, varies greatly coming from SW to ENE with the strongest winds from SSW to WSW and more moderate winds from NNE to ENE. The prevailing wind direction shows little variation during the summer months, from May to October, with weak winds approaching from NW to N. In November and December weak winds are coming from N to NE with stronger winds approaching from SW and W.

There is a daily pattern with the strongest winds occurring in the afternoon (12 am – 17 pm) and the weakest at night. The strongest winds come from SW and W and do not contribute to create waves that approach the shoreline but may play an important role in the mixing and circulation of lagoon water.

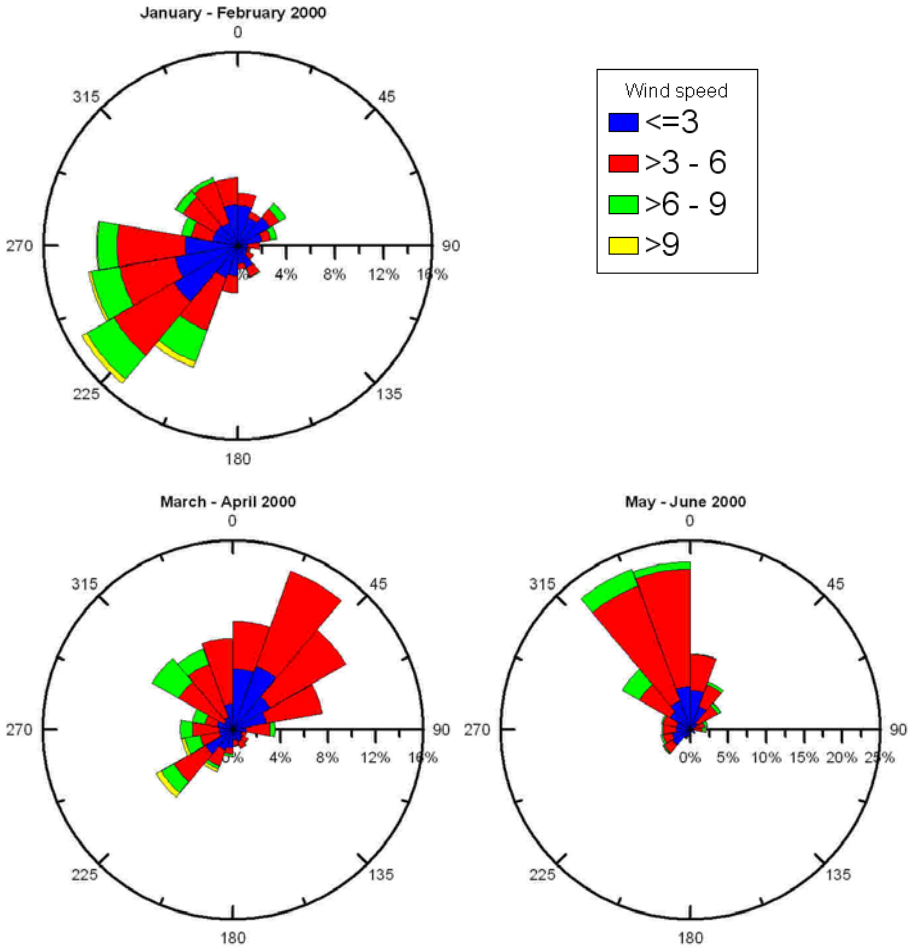

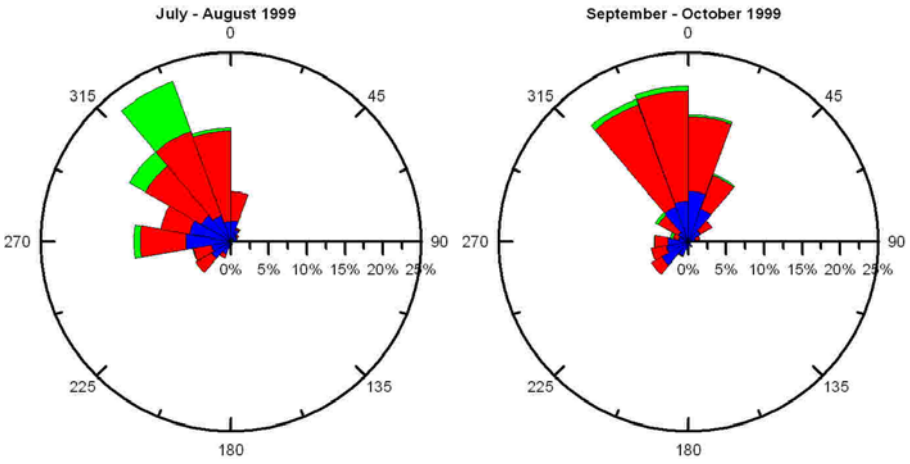

Figure 8: Bimonthly wind roses (m/s) for winds measured at Port Said from July 1999 to June 2000. November and December are missing due to gaps in the data.

Winds blowing over a water surface exert a horizontal force on the water surface. The force induces a surface current which leads to wind-induced waves as well as wind setup and setdown. Setup and setdown refers to the rise of water level on the downwind side and fall of water level at the upwind side respectively. The phenomena primarily occur in shallow water since the horizontal currents are retarded (US Army Corps of Engineers, 1984).

3.2 Wave climate

According to Frihy et al. (2002), the wave climate at the study area can be divided into three seasons, each varying with respect to the wind intensity and direction. During summer, from June to September, wave heights rarely exceed 1.5 m and the dominant wind direction is WNW. Waves are much higher during winter, November to March, coming primarily from N, NNW, and NW. The dominant northwestern winds are responsible for generating longshore currents in an easterly direction. During spring, April to May, the wind direction is reversed coming from N, NNE, and NE, creating a longshore current towards the west. Throughout the year the average wave height and period are 0.5 m and 6.3 s, respectively (Frihy, et al., 2002). In a study performed by Inman et al. (1984), it was concluded that the prevailing deep-water direction for storm waves is N60°W and that the wave period typically is from 8 to 10 seconds.

Wave measurements from a wave gauge located at Port Said have been studied. The recordings were made between 1999-08-24 and 2000-06-28 at a depth of 6.3 m. The data consist of 2436 recordings with three hours interval. The wave gage recorded the wave direction, period (T_Z), average spectral wave height (H_{m0}), and peak spectral period (T_P). The period T_Z is a good approximation of the mean wave period, T_m, computed from the zero and second order moments. The significant wave height, H_s, the average height of one-third of the highest waves, correlates well with H_{m0} which is computed from the zero-order moment of the wave spectrum.

The dominant wave direction is from NNW and N (Figure 9). The maximum recorded wave height is 2.10 m, the average wave height 0.53 m, and the average wave period 3.35 s. However, these recordings are made in shallow water at Port Said and do not perfectly apply for the water area outside the Bardawil Lagoon.

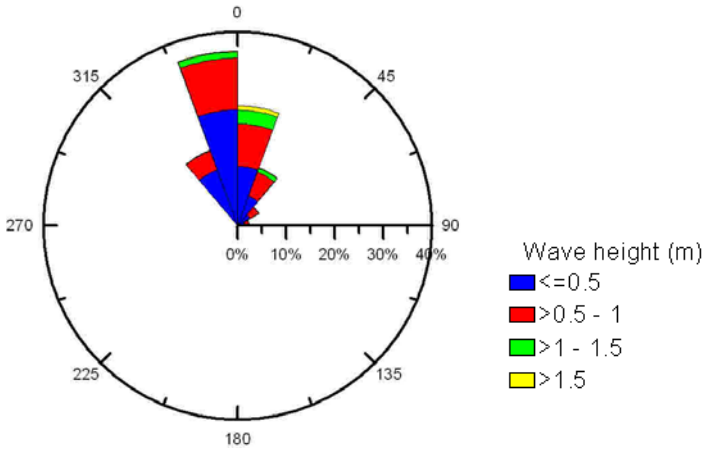

Figure 9: Nearshore wave rose at Port Said, 1999-08-24 to 2000-06-28, showing measured wave height and direction.

Offshore wave generation and propagation, as well as wave transformation in shallow water, are important processes that govern the longshore sediment transport, which is the responsible for inlet blocking. However, it is outside the scope of the present report to quantitatively investigate or examine the sediment transport and therefore waves are not considered in the modelling.

3.3 Water level fluctuations

The amplitude of the vertical rise and fall of the water level can vary greatly depending on the location. In the Mediterranean Sea the tidal changes are quite small due to the fact that a large volume of water is entrapped with only a narrow inlet connecting the water mass with the Atlantic Ocean (US Army Corps of Engineers, 1984). Besides the astronomical forces the tidal dynamics is affected by earth's rotation, bottom topography, shape of the shoreline, and bottom friction. The main tidal constituents at the north Sinai coast are M2 (lunar) and S2 (solar), which both are semi-diurnal components (Abdallah, et al., 2006). These components give rise to two high and low tides per day, *i.e.*, the tidal period is about 12 hours. The area is also classified as micro-tidal which mean that the difference between ebb and flood is less than 2 meter (Frihy, et al., 2002).

According to Inman et al. (1984) "the effect of tides is negligible except near large lagoons, where together with wind and evaporation they control water exchanges through the entrances." Inman et al. estimated the tidal range to 30 cm along the coast of the southeastern Mediterranean Sea (Inman, et al., 1984). In another study, performed by Frihy et al. (2002), the mean high- and low-water levels were measured

at El Arish, east of Bardawil Lagoon, and were found to be 20.22 cm and -11.01 cm, respectively, with a tidal range of 31.23 cm.

Available tidal data were measured at the east port in Port Said starting 1999-04-27 and ending 2000-05-04. Unfortunately, the hourly measured data have several gaps, some only a few hours others lasting for days. From the software WxTide (Flater, 2007) predictive tidal data was extracted and used to compare with the measured data. The results can be seen in Figure 10 and show a marked dissimilarity in amplitude between the data sets, while frequencies are similar. Some of the discrepancy is because the measured signal contains influences from other forces than the tide (*e.g.*, wind). Since the measured signal contained other types of forcing and had significant gaps, WxTide was employed for tidal predictions in this report in spite of the differences in amplitudes observed.

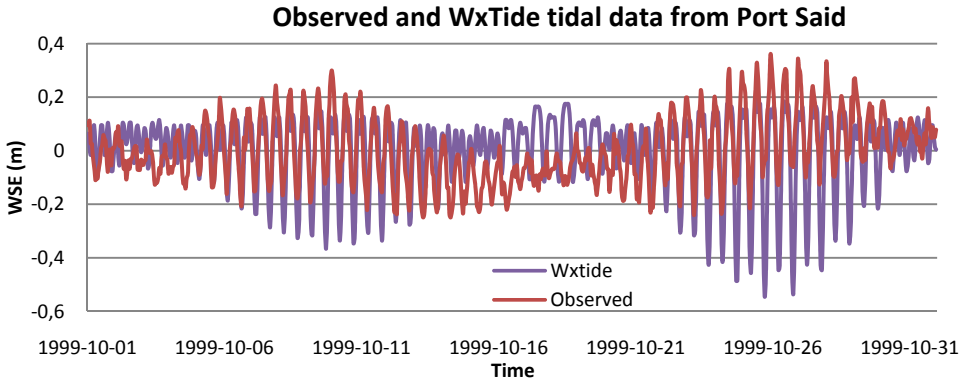

Figure 10: Observed and extracted (from the software WxTide) tidal data from Port Said in October 1999.

3.4 Sediment transport patterns

Coastal areas can be divided into compartments containing a complete cycle of sedimentation, including sources, transport paths, and sinks. Such compartments are known as littoral cells and their configuration is greatly dependent on the coastal type (Inman, 2005).

The coastline of north Sinai is classified as a marginal sea coast and is a part of the Nile Littoral Cell. Marginal sea coasts are characterized by limited fetch length and reduced wave energy due to the small water body that often fronts the coastline. The Nile Littoral Cell stretches a distance of approximately 700 km, from Alexandria west of the Nile Delta to Akko, Israel. Prior to the construction of the High Aswan Dam sediment was supplied by the Nile River. At present, sediment particles settle in the dam and the source of sediment comes from erosion of the Nile Delta instead. The Nile Delta is divided into two main branches known as Rosetta and Damietta where the Rosetta promontory is the main sediment source with an erosion rate estimated to 10 million m^3/year. The eroded material from the Nile Delta is moved by littoral transport along the coast.

The definition of littoral transport is the movement of sediments in the nearshore zone by waves and currents. Littoral transport can be divided into two different processes; longshore transport and cross-shore transport. The longshore transport is parallel and the cross-shore transport is perpendicular to the shoreline (US Army Corps of Engineers, 1984).

Longshore transport of sediment takes place as breaking waves stir up the sediments and then move them in the alongshore direction as a result of the dissipated wave energy and the longshore currents generated by the breaking waves. The direction of wave approach and wave crest angle determine the direction of the longshore transport, which as a result can reverse its direction from season to season, day to day, or even hour to hour (US Army Corps of Engineers, 1984).

The Nile sediments are transported in an eastward direction due to the currents from the Mediterranean gyre (Inman, 2005). East of the Damietta promontory the main driving force of the sediment transport is not the gyre, but longshore currents. These currents have an eastward direction as the dominant wave direction is from the W to N quadrant (Frihy, et al., 1997).

The general sediment transport patterns on the north Sinai coast, east of the Damietta promontory, can be seen in Figure 11. The area is divided into two littoral subcells known as the Port Said and the Bardawil subcells. Each subcell consists of a sediment source, an area where sand is eroded, and a stretch of coast where sand is accreted. Along the north Sinai coast the net sediment transport have the same direction, namely to the east (Frihy, et al., 1997).

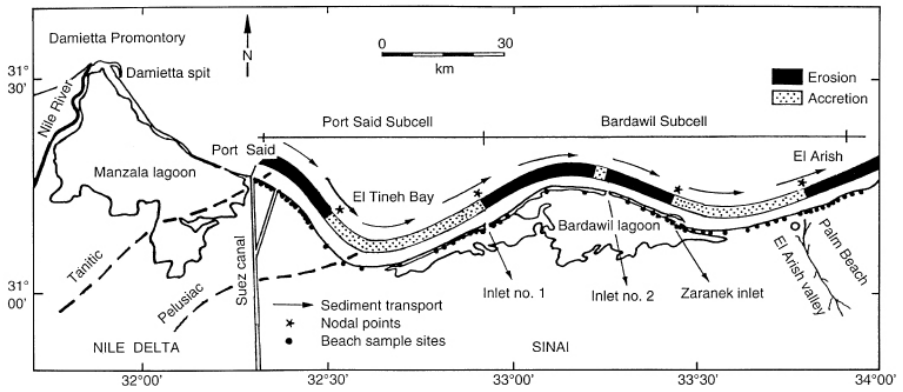

Figure 11. Erosion and accretion patterns. Sediment transport directions are shown by arrows. Modified after Frihy et al. (1997).

East of the Port Said headland erosion takes place, followed by accretion at El-Tinah Bay. The accretion continues on the sand barrier west of the western inlet of Bardawil Lagoon. This cycle of erosion and accretion defines the Port Said subcell (Frihy, et al., 1997).

In between the inlets, the central bulge of the Bardawil barrier is subjected to erosion which continues east of the eastern inlet. The Bardawil subcell ends with accretion of sediment at the El Arish embayment (Frihy, et al., 1997).

3.5 Inlet morphology changes

The longshore sediment transport can be either positive or negative depending on the wave direction. The sum of the positive and negative components is known as the net drift and the gross drift is the sum of the drift magnitudes. At unjettied inlets the drift direction is most likely of no importance, and the amount of dredging needed is depending on the gross drift, whereas the net drift can be zero (US Army Corps of Engineers, 1984).

Estimations of the net longshore sediment transport rate along the Bardawil subcell have been carried out by using the C.E.R.C formula (Vinja (1970), Suez Canal Authority (1983), and Emanuelsson, et al., (2007)) as well as by studying aerial photos of the sand erosion and accretion at the inlets (Inman, 1970) (Table 1).

The studies performed by Vinja (1970) and Inman (1970) both estimated the sediment transport rate of the east inlet to be about twice as large as for the western inlet. The difference in transport rate is explained by the relation between the wind and wave direction and azimuth angle of the barrier (Klein, 1986). The azimuth angle of shore normal of the western side of the barrier is 345° and the eastern side 18° (Emanuelsson, et al., 2007). As a consequence the longshore current is more frequent on the eastern side (Klein, 1986). However, the results from the Suez Canal Authority (1983) indicated the opposite relationship with a higher transport rate at the western inlet. This shows the existing uncertainty concerning the magnitude of the sand transport along the coast.

Table 1: Net and gross sediment transport at the west and east inlet at Bardawil Lagoon (Fanos, et al., 1994).

Study	Direction	West inlet (m^3/yr)	East inlet (m^3/yr)
Inman, 1970	Net E	300 000	500 000
Vinja, 1970	Towards E	340 000	600 000
	Towards W	140 000	100 000
	Net E	200 000	500 000
	Gross	480 000	700 000
Suez Canal Authority, 1983	Towards E	576 000	360 500
	Towards W	149 500	54 500
	Net E	426 500	306 000
	Gross	725 500	415 000
Emanuelsson, et al., 2007	Net E	40 000	258 000

The sedimentation imbalance of the north Sinai coast, described in section 3.4, is most pronounced at the man-made inlets. West of the western jetties, which were built to prevent shoaling of the inlets, sand is deposited (Frihy, et al., 1997). However, sand is still deposited at the inlet entrances and then moved by waves into the inlets. As a consequence, the sediment budget changes, leading to strong erosion east of the inlets creating movable sandbars which change the inlet morphology (Klein, 1986). Also, it causes a southward retreat of the sandbars east of the inlets (Fanos, et al.,

1994). The inlet morphology changes have been more dramatic at the east inlet where for example the coastline retreated 300 m between 1971 and 1978. During the period 1969 and 1978 the corresponding retreat at the west inlet was 180 m. The depth in the inlets has altered with the dredging campaigns, which have been inconsistent over the years (Klein, 1986).

In order to stabilize the inlets, to prevent spit bar formation, and to promote the exchange of water new jetties were constructed around 1995. In conjunction with the construction two channels were dredged. The coastline change between 1991 and 1999 can be seen in Figure 12 (west inlet) and Figure 13 (east inlet). New jetties are part of the displayed 1999 coastline. As noted previously, changes have been more dramatic at the east inlet with a coastline retreat of almost 200 m east of the inlet. The morphology and angle of the opening at the east inlet have changed after the construction of the new jetties, while at the west inlet they have stayed rather intact (Coastal Research Institute, 1971-1999). The latest dredging works of the inlet channels were performed in 2004 (Dr. Madhat, 2008).

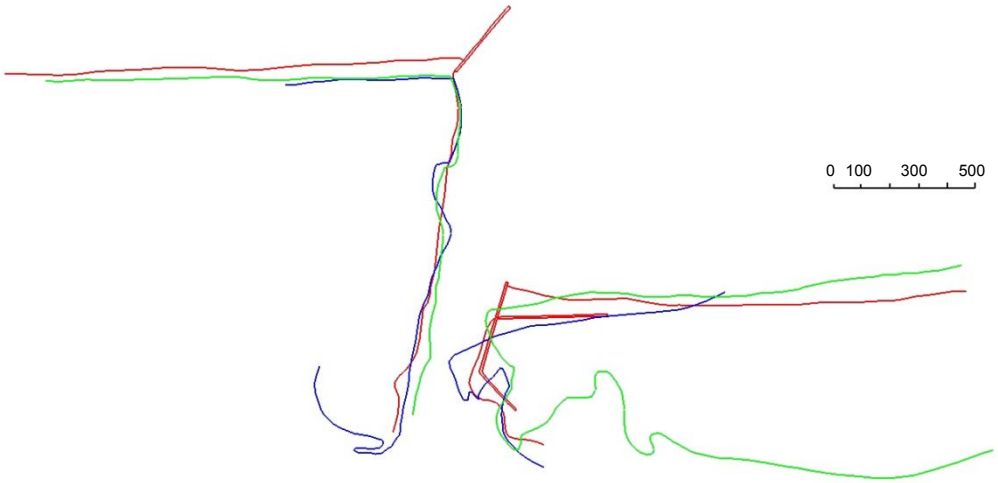

Figure 12: Coastline changes from 1991 through 1999 for west inlet. Red – 1999, Blue – 1994, Green – 1991, unit in meters. Modified after original (Coastal Research Institute, 1971-1999).

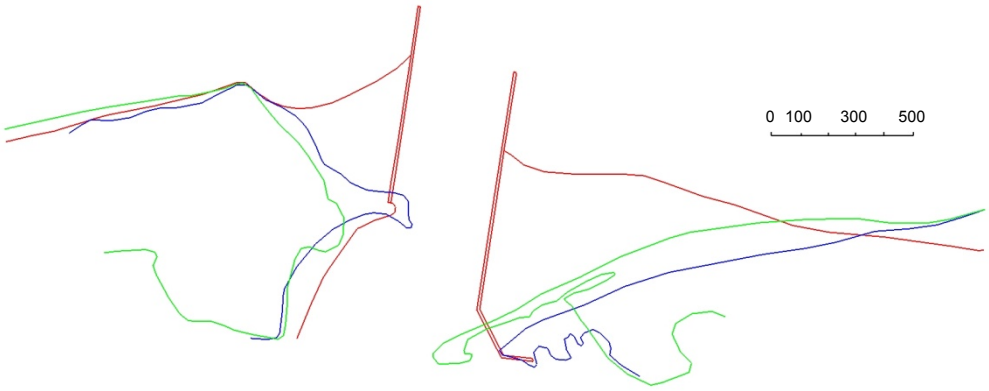

Figure 13: Coastline changes from 1991 through 1999 for east inlet. Red – 1999, Blue – 1994, Green – 1991, unit in meters. Modified after original (Coastal Research Institute, 1971-1999).

4 Physical processes in lagoons

The basic condition for lagoon formation is the abundance of sediment that can form a barrier or islands which protects the lagoon from the ocean. Barriers that entrap a water body, thereby creating a lagoon, can be formed in two main ways: flooding of lowland areas by sea level rise and spit formation, which embay the coastal shore. The flooding model is most common in areas where a drainage basin discharges into the ocean. This gives the lagoon a constant input of fresh water making the lagoon water brackish. Such lagoons, *e.g.*, Idku, Burullus and Manzala, are present in the Nile Delta. (Lagoon, 2008)

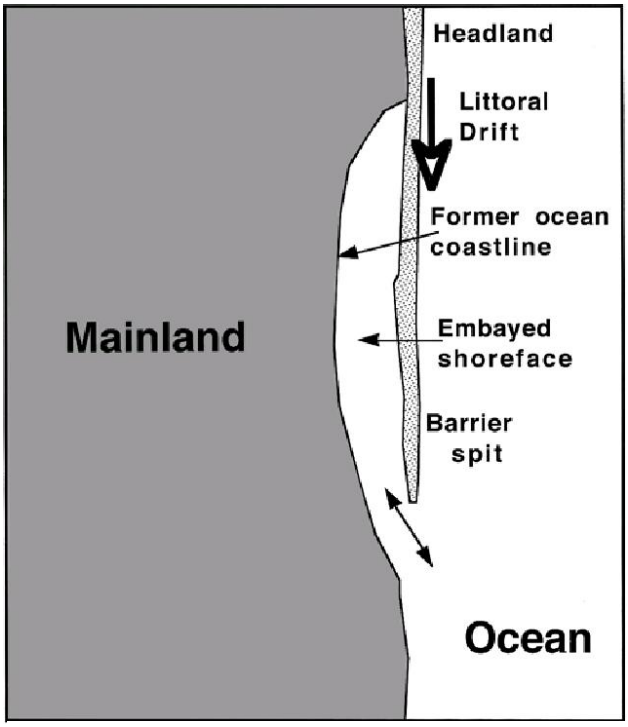

Figure 14: Lagoon formation according to the spit-embayment model (Oertel, 2005)

The spit-embayment model is most probable along coasts that are dominated by waves, as the north Sinai coast. The littoral drift build a sand barrier, spit, parallel to the shoreline creating an entrapped water body between the spit and main coastline (Figure 14). Due to the washover by waves, the backside of the spit often has an irregular shape compared to the straight form of the barrier outside and the mainland (Lagoon, 2008).

4.1 Water circulation

Tidal motions are an important driving force for the circulation of a lagoon. Apart from the tide the wind may play an important role in creating high and low sea water levels, which control the circulation and exchange of water through the inlets (Miller, et al., 1990). Large volumes of water either have to enter or exit the narrow inlets of the lagoon leading to strong currents around the inlets. Currents are weaker in the rest of the lagoon area resulting in sediment deposition and flat formation. Depending on the lagoon size, location, and area of contact with the ocean, the water residence time can vary greatly, from one week up to four years (Troussellier, 2007).

The internal circulation of a coastal lagoon is governed by both local and non-local forces. Local forcing by wind stress creates a downwind flow regardless of the wind direction. Water levels will experience a setup along the downwind shore and a

setdown along the upwind shore. The level of setup and setdown will depend on the magnitude of the wind stress, fetch length within the lagoon, and the water depth. As a response to the downwind water level setup a barotropic pressure gradient is established. This gradient gives rise to an upwind return flow, which takes place in deeper water. The return flow is primarily resisted by bottom friction forces. Non-local forces are mainly due to the tide, which causes variations in coastal sea level and forces water through the inlets. This action contributes to the circulation within the lagoon (Miller, et al., 1990).

Due to the large ratio between water surface area and depth, lagoons are often strongly affected by the interaction with the atmosphere. In warm regions there can be an imbalance between evaporation and fresh water input leading to hypersaline conditions in the lagoon. This is the case in Bardawil Lagoon which totally lack connection with any fresh water supply except the scarce precipitation (Lagoon, 2008).

4.1.1 Water balance

To understand the processes that maintain the chemical characteristics of Bardawil Lagoon the net water balance must be analysed. The water balance is a continuity, or mass conservation equation (Miller, et al., 1990), that describes the different fluxes that impact the water level in the lagoon. For coastal lagoons in semi-arid or arid regions, the tidal component is the principal variable and often many orders of magnitude larger than the other fluxes (Kjerfve, et al., 1996) on a tidal time scale. A general equation for the long-term water balance is given by (Miller, et al., 1990) and (Kjerfve, et al., 1996):

$$\frac{dV}{dt} = P - E + D + G + R \qquad \text{Equation 1}$$

In Equation 1 the fluxes are expressed in $m^3\ s^{-1}$ and a positive sign indicates gain of water and a negative sign loss of water. The left side of Equation 1 describe the change in storage over time, where V is the total volume of the lagoon.

The precipitation rate onto the lagoon is denoted P. The distribution of rainfall during the year is heterogeneous and most of the rain falls in the months of October to May (El-Bana, et al., 2002). The evaporation rate is E, which can be assumed to be homogenously distributed over the year, and D is the fresh water discharge from the drainage basin. In this arid desert landscape, almost completely void of hard surfaces, the discharge of fresh water is assumed to be zero as any rainwater precipitating on the desert sand either instantly evaporates or percolates into the soil (Coastal Research Institute, 2008). However, there are indications that some water is discharged from nearby agricultural lands and small communities (ramsar.org, 1991), however, due to lack of data the discharge is set to zero. The ground water flux into the lagoon is G. Due to the arid climate and low rainfall, the net groundwater exchange with the lagoon is very low, estimated to be 0.024 million m^3/day (Coastal Research Institute, 2008). In the calculations, G is set to zero.

Finally, R is the long-term residual advective gain or loss of water through a transverse cross-section (the inlets). The flux is the residual water exchange between the inflow of sea water and the outflow of lagoon water on long time scales (Kjerfve, et al., 1996).

Taking the above assumptions into consideration, Equation 1 can be rewritten as:

$$\frac{dV}{dt} = P - E - R \qquad \text{Equation 2}$$

On a longer time scale, the mean lagoon water volume can be assumed to be constant from one year to the next (Kjerfve, et al., 1996), and the effect of tidal water is zero, implying that the net flux through the inlets (R) can be estimated as the difference between evaporation and precipitation in Equation 2, which is illustrated in Figure 15 and given by:

$$R = P - E \qquad \text{Equation 3}$$

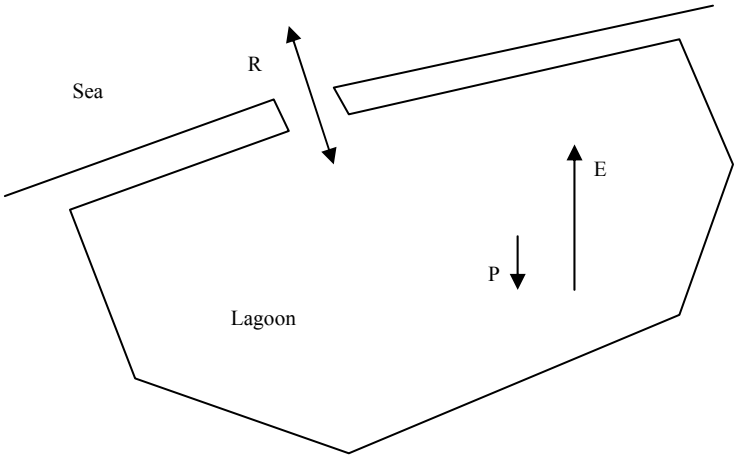

Figure 15: Schematic drawing of a lagoon with a single inlet describing long term advective transport Equation 3 in and out of the lagoon.

4.1.2 Lagoon flushing

Lagoon flushing is a concept that quantitatively describes the exchange rate, turnover or residence time. It is widely used in order to evaluate the lagoon water quality and management. On a tidal timescale (12 hours in the present case) the net volume change is significant and is largely dependent on tidal changes in the surrounding sea (Kjerfve, et al., 1996). This requires the insertion of a new term into Equation 2, T which represents the oscillating water flux on a tidal time scale:

$$\frac{dV}{dt} = P - E - R + |T| \qquad \text{Equation 4}$$

The inter-tidal volume during a tidal cycle (12 hours) is mathematically described as the tidal range in each segment multiplied with the area of the segment. That is, the volume is defined as the volume contained between the plane of low water (H_{ebb}) and

the plane of high water (H_{flood}) during a tidal cycle (Pritchard, 1960). This volume of water is described as the inter-tidal volume, $\Delta iV_{n,(t)}$,

$$\Delta \boldsymbol{iV_{n,(t)}} = \left(\boldsymbol{H_{flood} - H_{ebb}}\right)_{\boldsymbol{n}} \cdot \boldsymbol{A_n} \qquad \textbf{Equation 5}$$

where n is the segment number and t is the time step.

In order to determine a reference level, mean low water (MLW), water surface elevation data for the entire lagoon for an extended time period must be examined and the minimum water level during this time period is set to MLW (Figure 16).

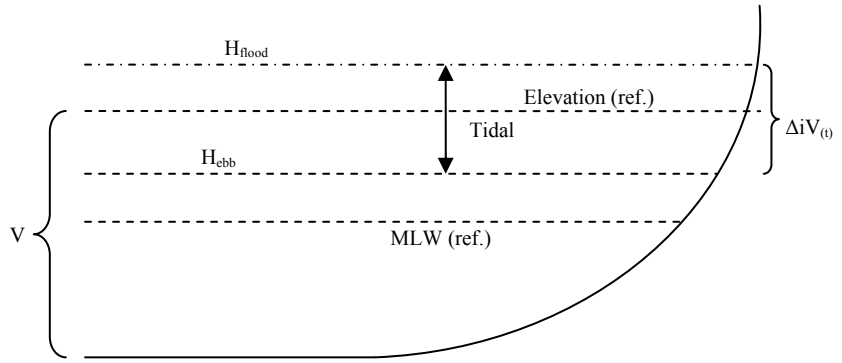

Figure 16: Inter-tidal volume $\Delta iV_{(t)}$, maximum flood volume V, reference levels MLW, and elevation in relation to the tidal water level in one segment at one specific time step.

Due to the spatial distribution of the segments and the progressive feature of the tidal wave, the time of high water in a segment will occur at different times throughout the tidal cycle (12 hours). Thus, the net inter-tidal volume cannot be calculated by simply summing the inter-tidal volumes since they occur at different times for each segment (Pritchard, 1960). Instead, the volume of each element, above MLW, at each hour of the tidal cycle is summed (Equation 6):

$$\Delta \boldsymbol{V_{(t)}} = \sum_{\boldsymbol{1}}^{\boldsymbol{n}} \Delta \boldsymbol{V_{n,(t)}} + \Delta \boldsymbol{V_{n+1,(t)}} + \cdots \qquad \textbf{Equation 6}$$

This yields a table of data containing the time step in hours and the sum of the segment volumes at each time step. Thus the volume of water contained in the entire lagoon area above MLW is obtained as a function of time. Plotting $\Delta V_{(t)}$ versus time gives a graph with a sinusoidal shape (Pritchard, 1960):

$$\Delta \boldsymbol{V_{net}} = \boldsymbol{Max}\left(\Delta \boldsymbol{V_{(t)}}\right) - \boldsymbol{Min}\left(\Delta \boldsymbol{V_{(t+x)}}\right) \qquad \textbf{Equation 7}$$

The net inter-tidal volume is then described as the difference between the maximum volume, at time *t*, and the minimum volume occurring at time $t + x$, where x is the phase shift in hours between maximum and minimum water volumes (Pritchard, 1960). Incidentally, ΔV_{net} and T are the same.

The ratio of the net intertidal volume to the total volume of the bay represents the fractional change in volume (Equation 8):

$$\mathbf{k} = \frac{\Delta V_{net}}{\mathbf{V}} \ (\mathbf{tidal\ cycle^{-1}}) \qquad \textbf{Equation 8}$$

Since the ratio is time dependent, *i.e.*, on the tidal cycle, a simple estimation can be found simply by inverting the ratio. The number given represents the number of tidal cycles required to replace all the water within the lagoon, assuming that there is no mixing of new and old water.

4.1.3 Hydraulic-flushing replacement time

One of the most common ways to describe the turnover time for a coastal lagoon is by calculating the lagoon flushing-hydraulic replacement time, t_h (Miller, et al., 1990),

$$\boldsymbol{t_h} = \frac{\bar{V}}{Q_f} \qquad \textbf{Equation 9}$$

where $\bar{V}$ is the mean volume of the lagoon and Q_f is the net freshwater discharge which is the sum of the surface runoff (D), groundwater seepage (G), precipitation (P) and correction for evaporation (E). In the model area, D and G are both zero, thus Q_f becomes,

$$\boldsymbol{Q_f = P - E} \qquad \textbf{Equation 10}$$

which is also termed R (Equation 3).

From Equation 10, it is quite clear that there is a net flow into the lagoon since the evaporation is roughly twenty times larger than the precipitation on average. The lagoon flushing-hydraulic replacement time assumes no mixing of new water, and the closest analogy is the time it takes to fill a volume (V) with a net inflow (Q).

4.1.4 Renewal time

In theory, the entire body of water will never be replaced, mixing occurs of "new" water with present "old" water in the lagoon. Therefore, it is often practice to calculate the flushing half-time or renewal time, $t_{50\%}$. This concept describes the time it takes to replace half the water under the assumption that intense mixing occurs (Kjerfve, et al., 1996). The volume ΔV_{net} is described as a volume of water interchanged between the lagoon and the sea during a specific time period (one tidal cycle). Since $t_{50\%}$ should be expressed in terms of days rather than tidal cycles, the rate constant per day, r_v, is found by multiplying k by two due to the semi-diurnal tidal pattern.

First order kinetics (Pritchard, 1960) yields,

$$\frac{\boldsymbol{dV}}{\boldsymbol{dt}} = -\mathbf{r_v} \cdot \boldsymbol{V} \qquad \textbf{Equation 11}$$

where $\mathrm{r_v} = 2 \cdot \mathrm{k}$

The volume V denotes the volume of the lagoon. Integrating Equation 11 from the initial volume, V_0 at $t_0 = 0$ to the new volume, V_{new} at a new time $t_{50\%}$. Rather than utilizing volumes, it is also common practice to derive the flushing half-time based on

salt concentrations in the lagoon (Pritchard, 1960) and (Miller, et al., 1990), see section 4.2.1. The integration yields:

$$\int_{V_0}^{V_{new}} \frac{1}{V} \cdot dV = -\int_{t_0}^{t_{50\%}} \mathrm{r_v} \cdot dt$$

$$-\ln\left(\frac{\mathrm{V_{new}}}{\mathrm{V_0}}\right) = \mathrm{r_v} \cdot (\mathrm{t_{50\%}} - \mathrm{t_0}) \qquad \frac{\mathrm{V_{new}}}{\mathrm{V_0}} = 0.5 \quad \mathrm{t_0} = 0$$

Solving for the renewal time, $\mathrm{t_{50\%}}$ gives:

$$\boldsymbol{t_{50\%} = \frac{0.693}{r_v}\ (days)} \qquad \textbf{Equation 12}$$

The time it takes to renew 99% of the water is found when $\frac{\mathrm{V_{new}}}{\mathrm{V_0}} = 0.01$ yielding:

$$\boldsymbol{t_{99\%} = \frac{4.605}{r_v}\ (days)}$$

4.2 Salt balance

The salt distribution of the lagoon is dependent on the net freshwater flow, the tidal exchange, and the mixing by wind and tide action (Pritchard, 1960). It is important to understand the salt balance, not only from the salt perspective itself, but since salt transport is similar to other dissolved pollutants (Miller, et al., 1990). Typically, lagoons in arid regions suffer from salt and/or pollutant enrichment since freshwater inflow is substantially less than evaporation. During 1969 to 1973, a series of field measurements were carried out concerning the salinity of Bardawil Lagoon, where the lagoon was divided into eight different compartments (Fanos, et al., 1994). Using salinity data, a more accurate description of the lagoon renewal time can be established. Salt extraction within the lagoon was not taken into account.

During flushing through the inlets, both new water, which entered during the last tide, and old water that was present in the lagoon is flushed out (Pritchard, 1960). Thus the actual rate of renewal should be lower if salinity is taken into consideration, *i.e.*, salinity becomes a mean to track the temporal origin of each water particle.

4.2.1 Box model with evaporation and salinity

The basic principle for the box model outlined by (Pritchard, 1960) is that sea water flows into the bay, which bring with it salt. As the tide shifts, lagoon water with a different salt concentration flows in the reverse direction out of the same inlets. To describe this, a conservation equation for salt is needed,

$$\boldsymbol{\frac{d\bar{s}}{dt} \cdot V_L = Q_{in} \cdot s_{in} - Q_{out} \cdot s_{out}} \qquad \textbf{Equation 13}$$

where $\bar{s}$ is the average salinity of the lagoon, s_{in} and s_{out} are the inflowing and out flowing salt concentrations respectively, V_L is the volume of the lagoon, and Q_{in} and Q_{out} represent the flow of "new" water in and out of the inlets, respectively.

Assuming that the volume of the lagoon is constant on a long time scale and the residual flow due to evaporation and precipitation (R) has previously been established in Equation 3, the long-term net fresh water balance for the lagoon becomes,

$$\boldsymbol{Q_{out} = Q_{in} + R} \qquad \textbf{Equation 14}$$

which is also valid for $T_{out} = T_{in} + T_R$, where T_{in} and T_R describe the fraction of inflow and net freshwater inflow, respectively, divided by the total volume of the lagoon. Thus, $T_{in} = Q_{in} \cdot V_L^{-1}$ and $T_R = R \cdot V_L^{-1}$ in the unit day^{-1}.

Substituting these expressions into Equation 13 gives:

$$\boldsymbol{\frac{d\bar{s}}{dt} = T_{in} \cdot (s_{in} - s_{out}) + T_R \cdot s_{out}} \qquad \textbf{Equation 15}$$

Assuming that the salinity relationship between the lagoon and the sea is of first order yields:

$$\boldsymbol{s_{in} - s_{out} = n \cdot (s_{in} - \bar{s})} \qquad \textbf{Equation 16}$$

Combining Equation 14, Equation 15, and Equation 16 gives:

$$\boldsymbol{\frac{d\bar{s}}{dt}} = (T_{out} - T_R) \cdot n \cdot (s_{in} - \bar{s}) - T_R \cdot s_{out}$$

Rearranging produces:

$$\boldsymbol{\frac{d\bar{s}}{dt}} = n \cdot T_{out}(s_{in} - \bar{s}) - T_R \cdot n \cdot s_{in} + T_R \cdot n \cdot \bar{s} - T_R \cdot s_{out}$$

$$\boldsymbol{\frac{d\bar{s}}{dt}} = n \cdot T_{out}(s_{in} - \bar{s}) - T_R(n \cdot (s_{in} - \bar{s}) + s_{out})$$

$$\boldsymbol{\frac{d\bar{s}}{dt} = n \cdot T_{out}(s_{in} - \bar{s}) - T_R \cdot s_{in}} \qquad \textbf{Equation 17}$$

Since the salt concentrations are known, while assuming that the change in salt over a short period of time remains zero, *n* can be found, and the residual flow ratio T_R can be determined easily from precipitation and evaporation data ($T_R = (P - E)/V$). Thus, Equation 17 (Pritchard, 1960) can readily be solved for T_{out}, which represents the fraction of salt particles present being flushed from the lagoon every day, leading to,

$$-\ln\left(\frac{C}{C_0}\right) = T_{out} \cdot (t - t_0) \qquad \frac{C}{C_0} = 0.5 \quad t_0 = 0$$

where *C* is the number of salt particles present at any time and C_0 is the original concentration of salt in the lagoon. With this method, an approximate solution to the water renewal time can be found based on salt flux through the inlets.

The ratio of new water (r_n) is determined by:

$$\boldsymbol{r_n = \frac{T_{out}}{r_v}} \qquad \textbf{Equation 18}$$

5 Mathematical modelling of lagoon flows

5.1 2D-tidal model (ADCIRC)

ADCIRC is an advanced system used for solving equations of motion for a moving fluid with emphasis on long waves. It is used for solving regional problems rather than local and typical applications are tide modelling, wind driven circulation, and analysis of hurricane storm surge and flooding. ADCIRC can be run as either a two-dimensional (2D) or a three-dimensional (3D) model. The water elevation is obtained from the solution of the depth-integrated continuity equation and the velocity is obtained from the solution of the momentum equations. ADCIRC use the finite element method and the finite difference method to solve the equations in space and time (adcirc.org, 2008).

The ADCIRC model used in this investigation has already been applied with success to other project areas such as Shinnecock Bay (FHWA, 2008) and New Orleans during hurricane Katrina (ADG, 2006).

5.1.1 Domain and sub-domain grid

The calculation domain for a tidal model is typically vast and the environment is highly complex in terms of bathymetry, morphology, and other coastline characteristics. In order to fully resolve the main area of interest, *i.e.*, the lagoon and the inlets, a high-resolution grid is needed. Rather than imposing a highly detailed grid over the entire model area, a refinement algorithm is set up so that areas of interest receive higher resolution and the remaining area lower resolution. For this purpose, finite element methods are very suitable. They allow for great flexibility with its subdivision of the system in triangles varying in form and size (Ferrarin, et al., 2005). Finite element methods are often used to solve partial differential equations over complex domains. The solution is based on reducing complex differentials into approximate linear equations.

The ADCIRC grid (mesh) is comprised of a series of finite elements radiating out from the inlets. This allows higher resolution in the lagoon and around the inlets. The algorithm for the density function is described in Equation 19 and the resulting mesh in the domain is shown in Figure 17 and the sub-domain in Figure 18,

$$distance = \sqrt{((a-x)^2 + (b-y)^2)}$$

$$size = [shallow\ celerity]$$

$$scale = \sqrt{distance / \max distance}$$

$$\boldsymbol{finalsize} = \mathbf{max}\left(\mathbf{M}, (\mathbf{N} \cdot \boldsymbol{size} \cdot \boldsymbol{scale})\right) \qquad \textbf{Equation 19}$$

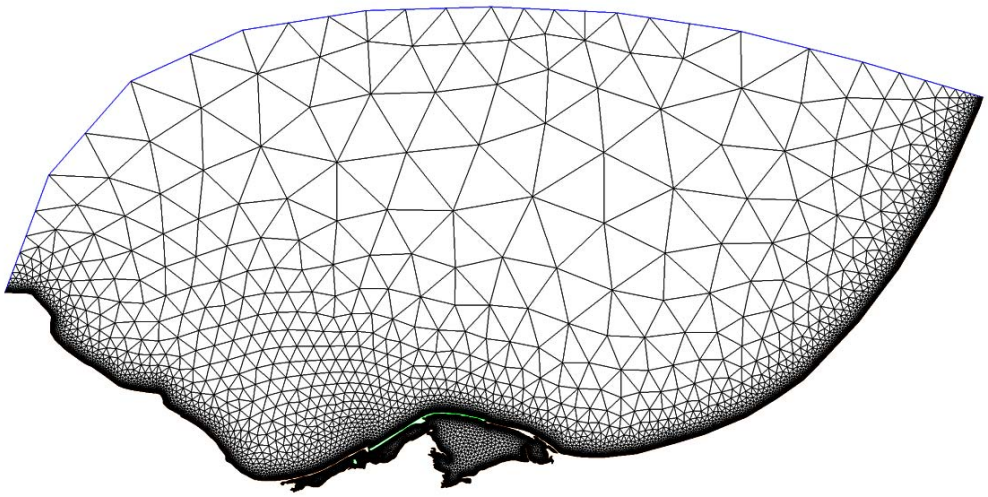

Figure 17: ADCIRC mesh of the model domain for the Nile littoral cell.

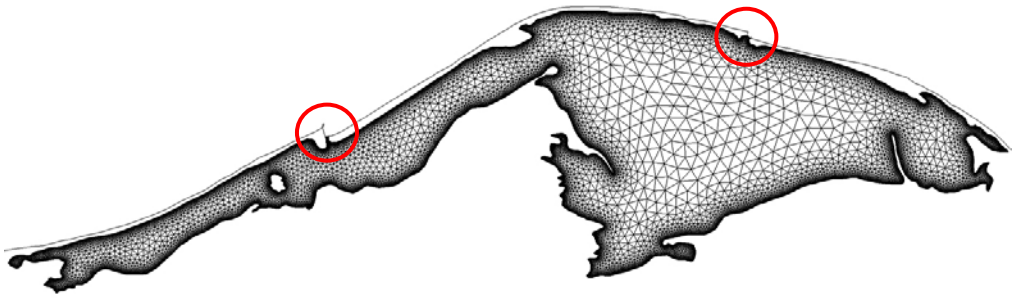

Figure 18: ADCIRC mesh of the model sub-domain. Inlets are marked with circles.

where x and y are coordinates of the refine point set at the centre of an inlet and a and b are coordinates of any other point. Shallow wave celerity was determined using the data calculator in SMS. The $finalsize$ function determines how the distribution of element sizes will vary throughout the domain, M defines the minimum element size, and $\mathrm{N} \cdot size \cdot scale$, where N is a constant, computes how rapidly the elements will grow to the maximum element size. Finally, the element definition was smoothed using a built-in method of SMS that limits the size of adjacent elements so that an adjacent element is not greater than twice or smaller than half the current element.

5.1.2 ADCIRC finite elements

The tidal ADCIRC model is built up by a mesh comprised of triangular finite elements. Each element (Figure 19) contain nodes, numbered 1-3 counter clockwise around the element. The nodes contain various data such as bathymetry.

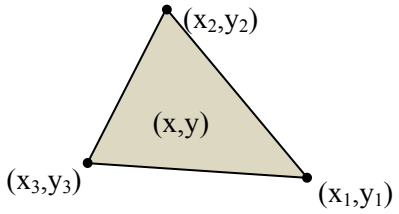

Figure 19: Illustration of a finite element and its coordinate locations.

Any variable, Y, can be expanded linearly within the element based on nodal values such that (Luettich, et al., 2004).

$$\Upsilon = \Upsilon_1\phi_1 + \Upsilon_2\phi_2 + \Upsilon_3\phi_3 = \sum_{i=1}^{3} \Upsilon_i\phi_i \qquad \textbf{Equation 20}$$

where Υ_i are nodal values of Υ at element node *i*, and,

ϕ_i are linear basis function defined as:

$\phi_1 = \frac{x_2y_3 - x_3y_2 + b_1x + a_1y}{2A}$, $\phi_2 = \frac{x_3y_1 - x_1y_3 + b_2x + a_2y}{2A}$, $\phi_3 = \frac{x_1y_2 - x_2y_1 + b_3x + a_3y}{2A}$

$a_1 = x_3 - x_2$, $a_2 = x_1 - x_3$ and $a_3 = x_2 - x_1$

$b_1 = y_2 - y_3$, $b_2 = y_3 - y_1$ and $b_3 = y_1 - y_2$

Furthermore, the area of each element is calculated as $A = \frac{b_1a_2 - b_2a_1}{2}$.

In ADCIRC solution files the nodal variable, Y, containing information that pertain to the change in water surface elevation (WSE) rather than the reference elevation in the default grid. At each time step in the solution, elements contain information with area and approximated WSE as well as volume.

5.1.3 Governing equations

ADCIRC utilizes the Generalized Wave-Continuity Equation (GWCE) to formulate the continuity equation. By solving the vertically-integrated continuity equation (Equation 21) the water surface elevation is obtained,

$$\frac{\partial \mathbf{H}}{\partial \mathbf{t}} + \frac{\partial}{\partial \mathbf{x}}(\mathbf{UH}) + \frac{\partial}{\partial \mathbf{y}}(\mathbf{VH}) = \mathbf{0} \qquad \textbf{Equation 21}$$

where

$U, V = \frac{1}{\mathrm{H}}\int_{-h}^{\varsigma} u, v\, dz$ = depth averaged velocities in x and y directions
u, v = vertically varying velocities in x and y directions
H = h + ς = total water depth
h = undisturbed water depth

ς = water level

The moment equations are given by:

$$\frac{\partial Q_x}{\partial t} + \frac{\partial UQ_x}{\partial x} + \frac{\partial VQ_x}{\partial y} - fQ_y = -gH\frac{\partial[\xi + P_s/g\rho_0 - \alpha\eta]}{\partial x} + \frac{\tau_{sx}}{\rho_0} - \frac{\tau_{bx}}{\rho_0} + M_x - D_x - B_x$$

$$\frac{\partial Q_y}{\partial t} + \frac{\partial UQ_y}{\partial x} + \frac{\partial Vy}{\partial y} - fQ_x = -gH\frac{\partial[\xi + P_s/g\rho_0 - \alpha\eta]}{\partial y} + \frac{\tau_{sy}}{\rho_0} - \frac{\tau_{by}}{\rho_0} + M_y - D_y - B_y$$

Where,

Q_x, Q_y = x, y- directed flux per unit width
D_x, D_y = x, y- directed moment dispersion
M_x, M_y = x, y- directed vertically integrated lateral stress gradient
B_x, B_y = x, y- directed vertically integrated baroclinic pressure gradient
τ_{sx}, τ_{sy} = imposed surface stresses
τ_{by}, τ_{by} = bottom stress components
ρ_0 = reference density of water
P_s = atmospheric pressure at the sea surface
H = vertically integrated lateral stress
η = Newtonian equilibrium tide potential
f = Coriolis parameter

The vertically-integrated momentum equations are substituted into the continuity equation to determine the depth-averaged velocities. For more information on the momentum equations and the theory behind the ADCIRC model see (Luettich, et al., 2004).

5.1.4 Time step selection

The purpose of deciding an appropriate time step is to reduce the simulation duration (*i.e.*, execution time). Underestimation of the time step results in unnecessarily long simulation run times, whereas overestimation leads to errors in the model calculations. This procedure is performed for both the tidal and circulation model (section 5.2.3).

To investigate the importance of selecting a suitable time step, observation points were located inside the lagoon (1), at the inlet (2) and at sea outside the lagoon at 20 meters depth (3). Residual water surface elevations (WSE) are displayed for 3 identical runs of ADCIRC in Figure 20 and Figure 21 using double time step increment at each run. The time steps are 4, 8, and 16 seconds. The relative difference is calculated as percent of water level at the same time stamp and observation point between 4 and 8 seconds (Figure 20) and 4 and 16 seconds (Figure 21).

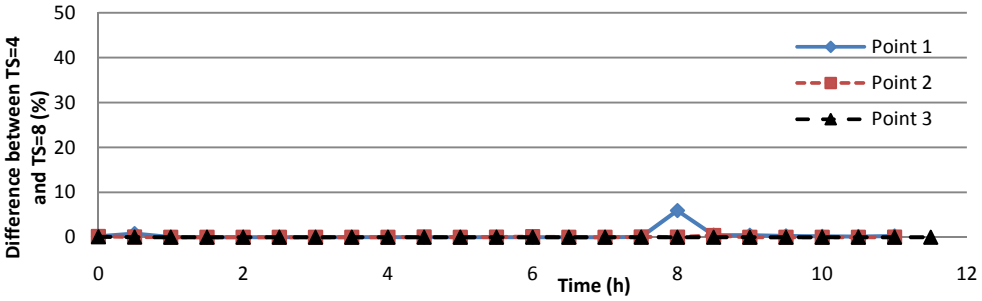

Figure 20: Relative difference in percent of water surface elevation calculated using ADCIRC for time steps of 4 and 8 seconds at 3 observation points. The y-axis shows the difference between the two time steps and the x-axis displays the time.

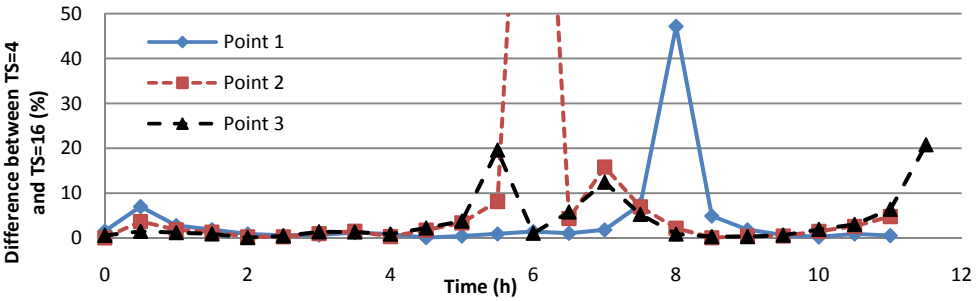

Figure 21: Relative difference in percent of water surface elevation calculated using ADCIRC for time steps of 4 and 16 seconds at 3 observation points. The y-axis show the difference between the two time steps and x-axis displays the time.

The results from ADCIRC time step analysis show that the relative difference between 4 and 8 seconds is minimal and within error margins. However, increasing the time step to 16 seconds greatly increases the error in WSE. The maximum error observed for point 2 is 147%, hence unacceptable. Based on this analysis, it is concluded that 8 second time step is an appropriate value for the time step in further model simulations.

5.1.5 Model input and settings

The grid imposed on the model area can be seen in Figure 17 and Figure 18. The minimum length of any element side is set to 25 meters and the maximum to 50,000 meters. The method of grid generation is a compromise between accuracy and calculation speed (Ferrarin, et al., 2005). The resulting grid contains 45543 nodes and 80642 elements.

For the greater Nile cell satellite images from Google Earth (Google, 2007) were used to create the coastline and the offshore bathymetry for the area was obtained from a public NOAA website (NOAA/NGDC&WDC for MGG Boulder, 2008).

For the lagoon itself, bathymetric data was provided by Coastal Research Institute in Alexandria, Egypt (Figure 2 and Figure 65 in Appendix). The survey of the lagoon was performed in 1971, while more recent studies of the inlets were available from

1996. In 2004 a study for the eastern inlet was done, but for conformity, this data has not been applied to the model. Since the lagoon barrier moves inward over time, the discrepancy of inlet locations between 1971 and 1996 has been subjectively fitted in order to create a complete functional coastline with inlets. Due to lack of data, the third inlet (Al-Zaranik), which is natural, located on the eastern fringe of the lagoon, is omitted from the model. This inlet is little importance for the overall water exchange of the lagoon since it is very shallow and never dredged.

The bathymetric data in the lagoon consists of contour lines and transect lines. The depth contours ranges from 0.5 to 2.0 meter, with 0.5 meter increment (Figure 2). The transect lines contain higher detail and are measured in centimetres (Figure 65). For the inlets (Figure 22), contour lines with 0.5 depth meter interval are available. Some manual fitting of the depth data has been made in order to obtain smooth transitions from the inlet data to the offshore and lagoon data.

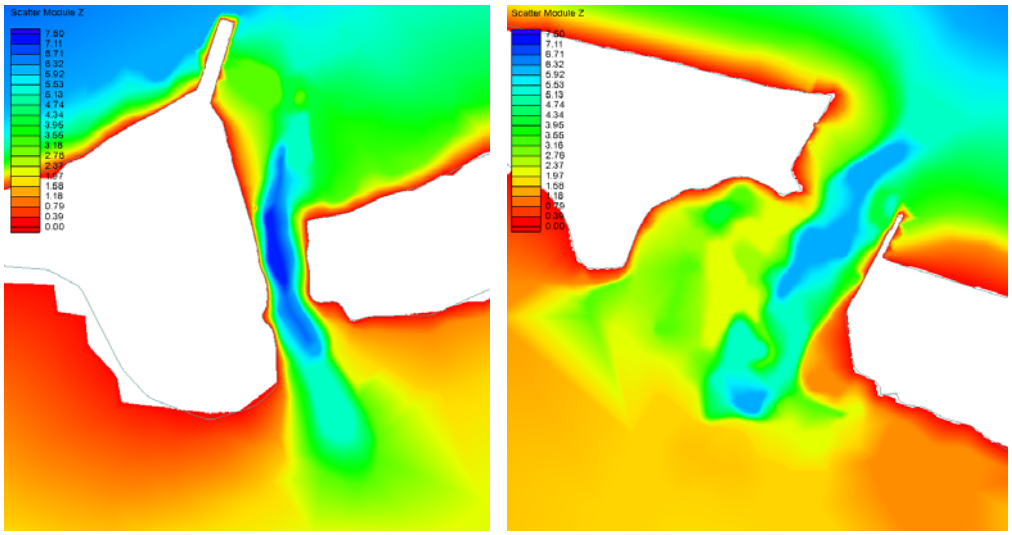

Figure 22: Bathymetry of western (left) and eastern (right) inlets in meters, interpolated between known values according to data obtained from Coastal Research Institute, Alexandria, Egypt.

The coastline was created using arcs, interconnected by vertices at 50 meter apart, and the elevation for the coastline was set to zero. Some areas were excluded from the model domain as they were regarded as insignificant for the overall exchange processes at the lagoon inlets. Furthermore, these areas are extremely shallow and situated at the fringes of the lagoon. Lack of data and problems estimating the actual depths are further reasons for this exclusion. In the offshore region of the Nile littoral cell, extensive data from NOAA (National Oceanographic and Atmospheric Administration) as depth contours, ranging from 10 to 1200 meters, were traced using arcs with the elevation set to the current line depth. The arcs were transformed into a scatter set and the depth in between the lines were determined using built in linear interpolation functions in order to create a smooth bottom contour (Figure 23). In the nearshore regions (0-10 meter), information about the depths at various locations is sparse and is only available around the inlets. The offshore contour lines are extended

along the entire barrier with the assumption that the slope in between the bottom contours near the inlets is representative for the length of the coastline.

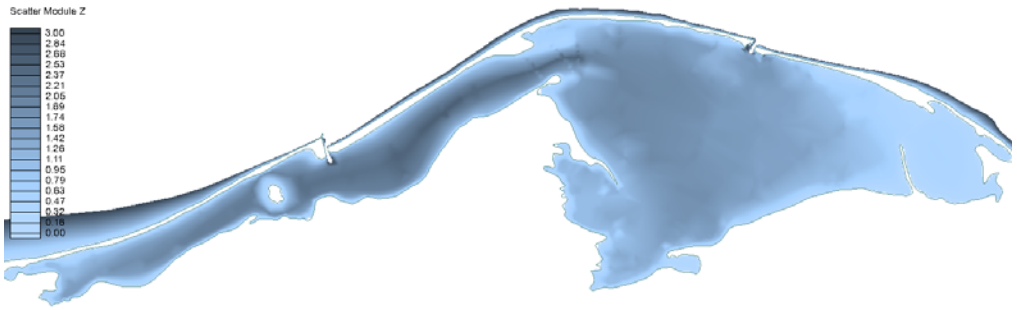

Figure 23: Bathymetry of the Bardawil lagoon in meters, interpolated between known values according to data obtained from Coastal Research Institute, Alexandria, Egypt.

Forcing for the ADCIRC model was obtained using data from tidal prediction software (WxTide) for two locations, namely Port Said and Tel-Aviv. The data series selected stretches from 1996-08-01 to 1996-09-30 to match the date of the inlet bathymetry maps. In ADCIRC, the forcing is applied as a boundary condition along the ocean boundary of the model domain. Since the matching of the tidal data from the two stations at specific time steps is low, the boundary condition was split into nine separate segments. At the west and east ends of the boundary segment, unedited Port Said and Tel-Aviv data were applied. For the seven intermediate segments, tidal data was mathematically interpolated so that the transition of data along the entire boundary became smooth. The raw data from WxTide at each segment is given with respect to a reference point (+0.64 m for Port Said and +0.21 m for Tel-Aviv), hence the data had to be normalised. In Figure 24, normalised forcing data, as extracted from WXTide, are plotted over time for the duration of the ADCIRC modeling. Interpolated forcing data on the seven intermediate boundaries is not shown in the figure.

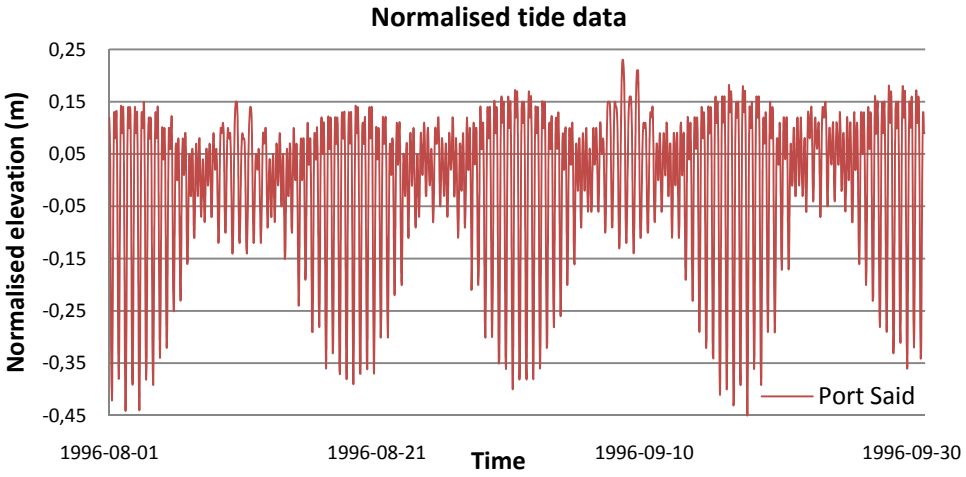

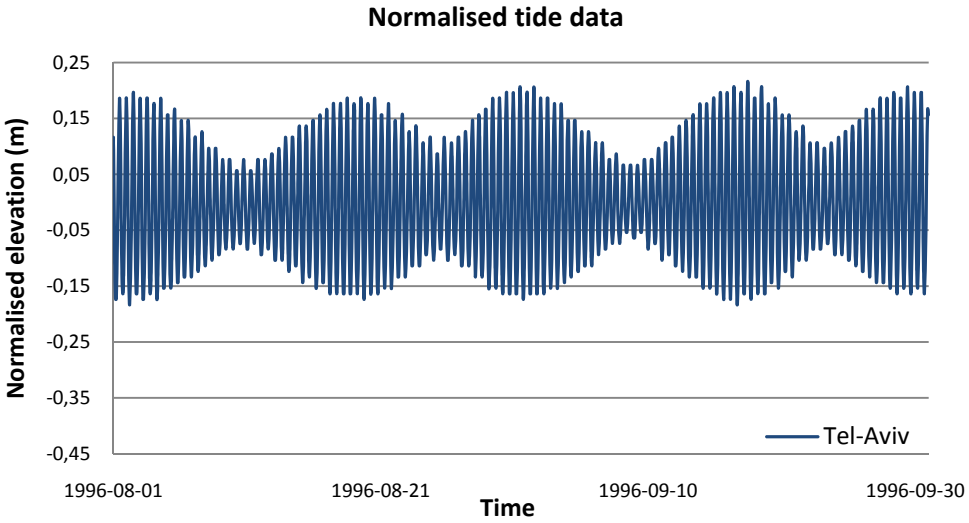

Figure 24: Hourly tidal forcing input data from WXTide (Port Said, top, and Tel-Aviv, bottom) for ADCIRC. Normalized water surface elevations on the y-axis and time on the x-axis.

A constant linear bottom friction of 0.0025 was applied in all model simulations, which is the default setting in ADCIRC and the Coriolis parameter was set to $1 \cdot 10^{-4}$.

Starting on the 1st of August in 1996 the ADCIRC model was run for 60 days, using a time step of 8 seconds, so that the semi-diurnal tidal pattern and several occasions of spring and neap tide were included within the run time (Miller, et al., 1990).

5.1.6 Data extraction and analysis

By means of segments

Extraction of volumetric elevation data from ADCIRC was done by splitting the lagoon itself into 17 segments (Figure 25). The method was originally developed by Pritchard while investigating Chincoteague Bay, MD, a lagoon of 328 km^2 divided into 16 segments (Pritchard, 1960).

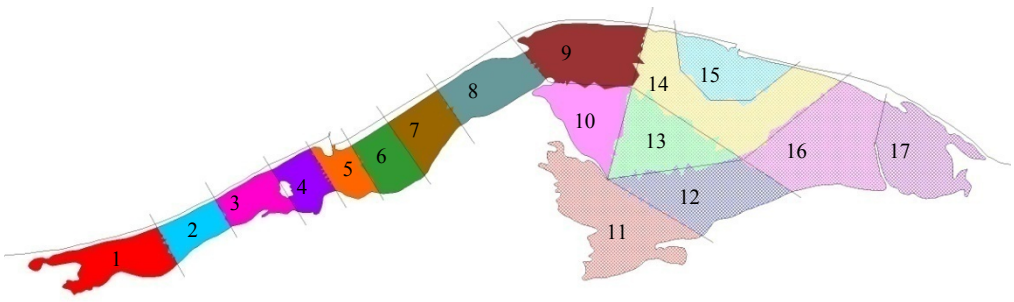

Figure 25: Bardawil lagoon divided into 17 segments.

The division into segments and the relative size of each segment has been made so that the majority of the elements within each segment experience simultaneous positive or negative changes in water surface elevation due to tidal action. At each time step, the total volume change in each segment is extracted from the model (Table 2). By merging elements into larger logical volumes, data extraction and analysis become significantly easier and less time consuming.

Table 2: Sample result of local volumes above MLW and net intertidal volumes.

	Volume above local MLW (10^6 m^3)			Total volume above local MLW (10^6 m^3)	Net intertidal volume (10^6 m^3)
Time (h)	Segment 1	Segment N	Segment 17		
823	0.43	...	0.45	13.70	-4.33
824	0.46	...	0.47	12.98	
...					
827	0.51	...	0.49	9.59	
828	0.50	...	0.47	9.38	5.82
829	0.48	...	0.46	9.75	
...					
834	0.46	...	0.47	14.84	
835	0.48	...	0.49	15.20	-4.10

The measured segment volumes are referenced to the local mean low water (LMLW) for each segment which is a reference water level that is the absolute low point during the entire simulation duration. Due to the progressive nature of the tide and the geometry of the lagoon, the time of occurrence for the LMLW differs from segment to segment. The corrected volume at each time step in each segment is referred to as *Volume above local mean low water*. The concept of *Net intertidal volume* is described by Pritchard as the difference between maxima and minima of sum of the volume above LMLW in each segment (Table 2). This volume describes the water which either enters or exits the lagoon during a tidal cycle. This method, which is mathematically described in section 4.1.3, was previously used to study the salt balance and exchange rate of Chincoteague Bay, MD, USA (Pritchard, 1960) as well as Lagoa de Araruama, Brazil (Kjerfve, et al., 1996).

Flow through inlets

Simple mass balance dictates that any changes in volume observed in the lagoon using Pritchard's method is caused by water flowing through the inlets. ADCIRC is capable of computing water particle velocities. Observation profiles are set up across each inlet, measuring the water velocity at 1-meter intervals (Figure 26). By integrating the water velocity along the transect multiplied at each interval by the corresponding depth, the total flow is obtained.

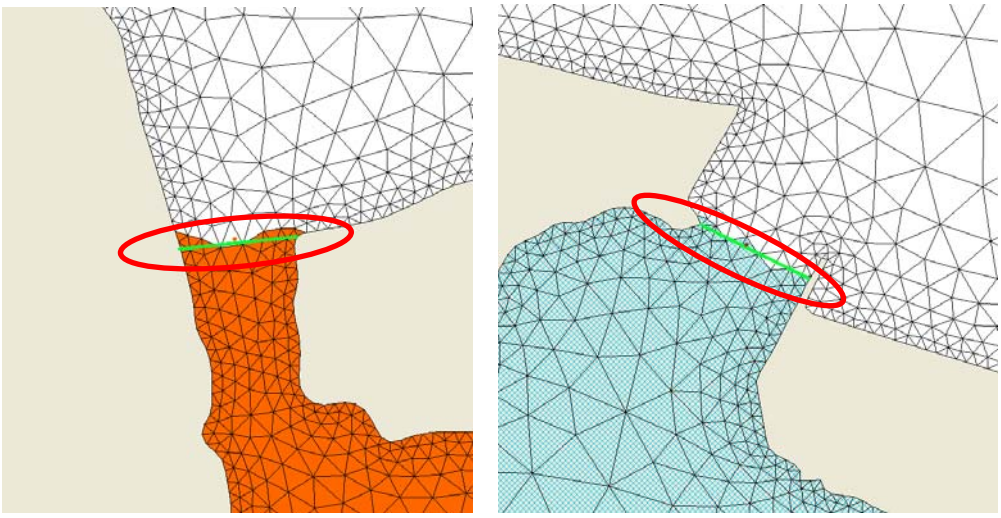

Figure 26: Observation profiles (green) across west (left) and east (inlet) marked with red circles.

Water flow data through the inlets have been collected for time periods corresponding to the tidal cycles investigated using Pritchard's method in order to compare the methods. The calculation of the inlet flows also allows us to examine the relative importance of each inlet in terms of the flow.

5.2 2D-Circulation model (CMS-Flow)

The Coastal Modelling System (CMS) is a computer modelling tool specifically developed for inlets on a local scale. It features multidisciplinary capacity to handle many variables such as water surface elevation, wind, and waves (Buttolph, et al., 2006). CMS-Flow is a finite-volume numerical representation of the two-dimensional (2D) depth-integrated continuity and momentum equations of water motion.

5.2.1 Domain and sub-domain grid

Grids in CMS-Flow are rectangular in shape and are created by defining a single or multiple refine points. For Bardawil lagoon, a refine point has been defined at the centre of each inlet for both the x and y-axis. The general characteristics of the grid are outlined in Table 3. Forcing for the CMS model is wind and extracted water surface elevation from ADCIRC. In Figure 27 the grid is shown with water cells in blue, inactive land cells in grey, and the forcing cell string in red. Forcing is exerted along the cell string.

Table 3: Numerical data of the Cartesian CMS grid.

Parameter	Value
Inlet, minimum cell size (m)	20
Grid, maximum cell size (m)	250
Growth factor (bias)	1.10
Depth (m)	From scatter set
Number of cells	84040

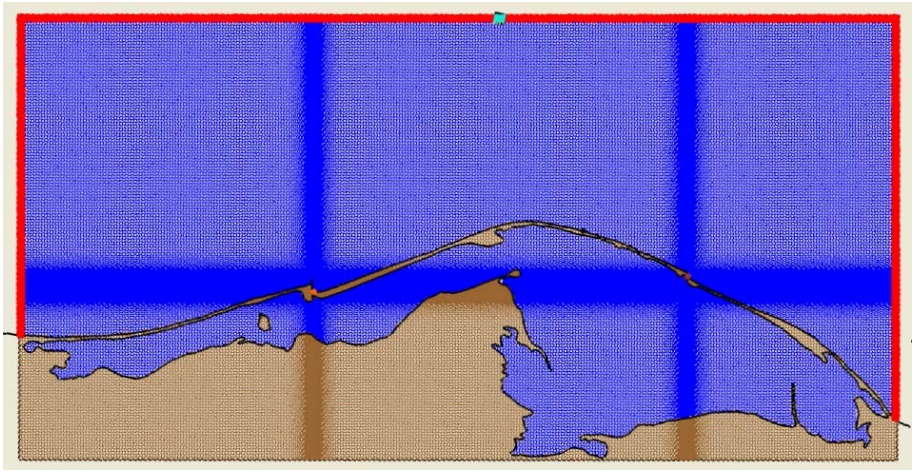

Figure 27: CMS-Flow finite volume grid for the lagoon and nearshore region.

5.2.2 Governing equations

In CMS-Flow the 2D depth-integrated continuity and momentum equations are solved by applying a finite volume method. Velocity components are calculated in two horizontal dimensions (Buttolph, et al., 2006). The equations are,

$$\frac{\partial(h+\eta)}{\partial t}+\frac{\partial q_x}{\partial x}+\frac{\partial q_y}{\partial y}=0$$

$$\frac{\partial q_x}{\partial t}+\frac{\partial u q_x}{\partial x}+\frac{\partial v q_x}{\partial y}+\frac{1}{2}g\frac{\partial(h+\eta)^2}{\partial x}=\frac{\partial}{\partial x}D_x\frac{\partial q_x}{\partial x}+\frac{\partial}{\partial y}D_y\frac{\partial q_x}{\partial y}+fq_y-\tau_{bx}+\tau_{wx}+\tau_{Sx}$$

$$\frac{\partial q_y}{\partial t}+\frac{\partial u q_y}{\partial x}+\frac{\partial v q_y}{\partial y}+\frac{1}{2}g\frac{\partial(h+\eta)^2}{\partial y}=\frac{\partial}{\partial x}D_x\frac{\partial q_y}{\partial x}+\frac{\partial}{\partial y}D_y\frac{\partial q_y}{\partial y}-fq_y-\tau_{by}+\tau_{wy}+\tau_{Sy}$$

where:

h = still-water depth relative to a specific vertical datum
η = deviation of the water-surface elevation from the still-water level
t = time
q_x = flow per unit width parallel to the x-axis
q_y = flow per unit width parallel to the y-axis
u = depth-averaged current velocity parallel to the x-axis
v = depth-averaged current velocity parallel to the y-axis
g = acceleration due to gravity
D_x = diffusion coefficient for the x direction
D_y = diffusion coefficient for the y direction
f = Coriolis parameter
τ_{bx} = bottom stress parallel to the x-axis
τ_{by} = bottom stress parallel to the y-axis
τ_{wx} = surface stress parallel to the x-axis
τ_{wy} = surface stress parallel to the y-axis

τ_{Sx} = wave stress parallel to the x-axis
τ_{Sy} = wave stress parallel to the y-axis

For further information regarding CMS-Flow and the governing equations, see the manual (Buttolph, et al., 2006).

5.2.3 Time step selection

In doing the sensitivity analysis regarding the selection of time step for CMS-Flow, a reduced grid is used for time-saving purposes. Points 1 and 2 are located at the same location as for ADCIRC analysis. However, point 3 had to be moved towards the shore since the model domain for CMS-Flow is smaller. Relative difference in WSE is computed in the same manner as for ADCIRC, but at different time steps. Three identical model runs were made using time steps at 0.5, 1.0, and 2.0 seconds. A fourth run was attempted at Ts = 4 seconds, but it could not be finished. Results are displayed in Figure 28 and Figure 29.

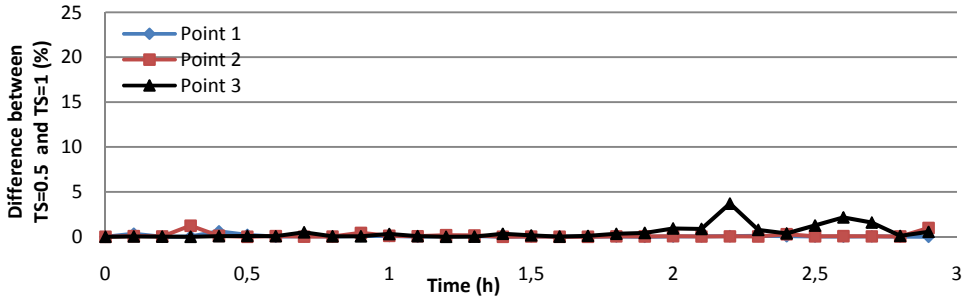

Figure 28: Relative difference in percent of water surface elevation calculated using CMS-Flow for time steps of 0.5 and 1 seconds at 3 observation points. The y-axis shows the difference between the two time steps and the x-axis displays the time.

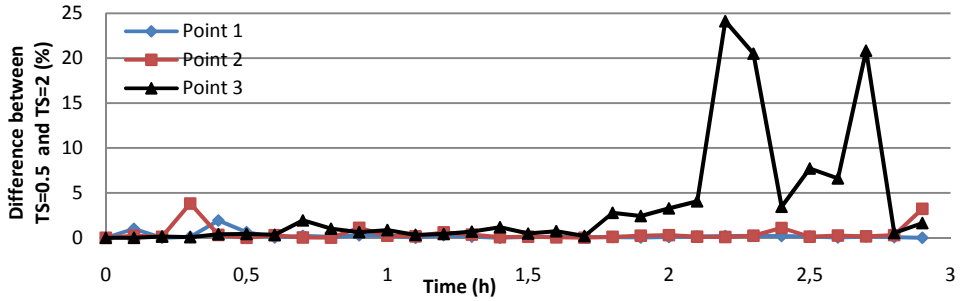

Figure 29: Relative difference in percent of water surface elevation calculated using CMS-Flow for time steps of 0.5 and 2 seconds at 3 observation points. The y-axis shows the difference between the two time steps and the x-axis displays the time.

As the model was unable to compute a solution for a time step of 4 seconds, the maximum time step possible was 2 seconds. Due to the ratio of cell sizes (smallest cell compared to largest cell) in the refined grid, a 2-second time step yields a warning in SMS, whereas a 1-second is stable without warnings. Furthermore, the

relative error between 2 and 0.5 second time step is unacceptable, particularly for point 3. Thus, the CMS-Flow model was run using a 1-second time step.

5.2.4 Model input and settings

The software mainframe, SMS, which houses both ADCIRC and CMS-Flow, is fully capable of working with layers. Hence, the same bathymetric data were used in both models. Observed wind data from the 1999 August-September period was applied in the model (see Figure 8). The predominant wind direction for this period was NNW-NW and average wind speed was 3.9 m/s. Tide forcing is applied to the domain through the cell string. At each cell on the string, tidal data for each time step is extracted from the ADCIRC model.

Starting on the 4st of August in 1996 the CMS model was run for 12 days, using a time step of 1 second. CMS-Flow requires more processing power than ADCIRC, and data to be analyzed by the model does not contain large-scale time patterns; thus, it was deemed unnecessary to run the model for the full 60 days.

6 Simulation results

In the following sections, 6.2 and 6.3, simulation results from the SMS software, using ADCIRC and CMS-Flow, are presented. In ADCIRC the tidal effect on the water surface elevation and flow through the inlets were studied. The wind effect was investigated with CMS-Flow as well as the combined effects of wind and tide together. A summary of simulations scenarios is presented in Table 4. With the tidal model two special case scenarios were performed to see how the lagoon reacts when one of the inlets are closed and to find out which inlet is the most important to maintain a good exchange of water with the Mediterranean Sea. Closure of either inlet may occur if the dredging stops. This last happened in 1970 when the east inlet was blocked by sediments (Klein, 1986). Results presented in the following sections relates to the standard state of the lagoon, when both inlets are open, unless otherwise stated. The simulation results were also used to calculate renewal times for each scenario and the internal circulation of the lagoon was studied in the CMS-Flow runs.

Table 4: Summary of simulation scenarios.

Scenario	Model	Inlets	Input
1	ADCIRC	Both	Tide
2	ADCIRC	West closed	Tide
3	ADCIRC	East closed	Tide
4	CMS-Flow	Both	Wind
5	CMS-Flow	Both	Tide
6	CMS-Flow	Both	Tide and wind

For a more detailed presentation of the input see sections 5.1.5 and 5.2.4.

6.1 General results

Before presenting the specific simulation results, general data and results from the simulations are presented in Table 5 and Table 6. Comparing the mean depth with previous studies (El-Bana, et al., 2002) the value is about 20-50 cm lower. The same result is obtained for the area, which is $40\text{-}90 \cdot 10^6$ m^3 smaller than the area in previous studies (Levy, 1974). This follows from the delimitation of the lagoon area in the model. There is a slight change in both the area and volume of the lagoon between the scenarios in ADCIRC, not presented, due to the fact that the coastline and bathymetry around the inlets have been modified. The two inlet cross-sectional areas are near identical: 1236 m^2 and 1191 m^2 for the east and west inlet, respectively.

Table 5: General data and results.

Parameter	
Area (10^6 km^2)	561
Volume at zero elevation (10^6 m^3)	689
Mean depth (m)	1.33

In order to understand the processes governing the water quality, the water balance and the residence time of the lagoon must be estimated. The effects of long-term processes, such as evaporation and precipitation, are in principal determined by the water balance for the lagoon disregarding tidal flushing. The negative sign on Q_f indicates the direction of the flow, *i.e.*, negative residual flow due to the high

evaporation rate. The results are presented in Table 6 where t_h is the lagoon flushing-hydraulic replacement time, which is determined from Equation 9.

Table 6: Results from applying Equation 9 (Miller, et al., 1990) to determine t_h, the lagoon flushing-hydraulic replacement time, based on macro-scale events, *i.e.*, evaporation and precipitation.

Parameter	Value
$\bar{V}$ $(10^6\ m^3)$	689
E $(10^6\ m^3/day)$	2.73
P $(10^6\ m^3/day)$	0.14
Q_f $(10^6\ m^3/day)$	-2.59
t_h $(days)$	266

6.2 ADCIRC

Simulations in the regional model ADCIRC were performed to investigate both the large-scale pattern of the tidal action and differences between the inlets, using a simulation time of 60 days. Three different scenarios were run: Scenario 1 refers to the standard state when both inlets are open, whereas in Scenario 2 and 3 the west and east inlet, respectively, are closed.

6.2.1 Water surface elevations inside the lagoon

The tidal forcing along the ocean boundary forces water through the inlets and the progressive action of the tide causes changes in water surface elevation throughout the lagoon. The change in WSE at three observation points in the lagoon is shown in Figure 30. The general shape of the curves is very similar to the tidal forcing in Port Said and Tel Aviv (Figure 24). However, the amplitude is significantly lower with a maximum value of about 16 cm at the east inlet compared to 50 cm at Port Said. The amplitude decreases with the distance from the inlets due to an attenuation effect of the tidal signal. At the observation point "inside lagoon" the changes in WSE are only a few centimetres. It can be observed that the amplitude of the WSE is lower at the west inlet than at the east (Figure 30).

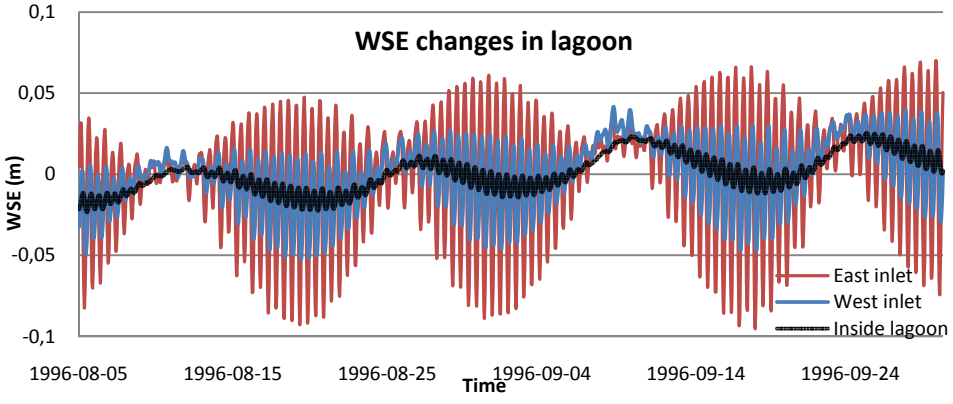

Figure 30: Water surface level changes at three observation points in the lagoon. The observation point "inside lagoon" is located in segment 12 (see to Figure 25 on page 34).

The total volume above local mean low water (LMLW), which is the sum of the volume above LMLW in each segment at each time step, was calculated and is presented in Figure 31. Four characteristic features can be identified in the graph: First, the general trend of increasing water volume with time. This trend is also present in the tidal data from Port Said and Tel-Aviv. Second, the large-scale sinusoidal pattern with a period of roughly 13 days. Third, the ripple-type feature caused by the semi-diurnal tide action is visible throughout the simulation. Fourth, the ripples dissipate halfway into each large-scale sinusoidal increase. During this period the flow through the inlets is significantly lower than during the semi-diurnal tide action. Instead the flow is unidirectional for a period of two to four days and the lagoon is mainly receiving water during this period.

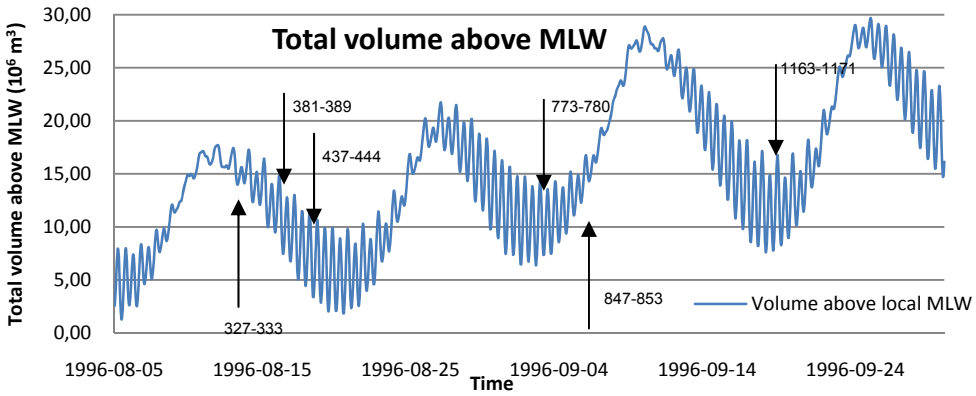

Figure 31: Total volume above local mean low water over time inside the lagoon with both inlets open. Arrows indicate selected tide prisms examined in Figure 38 and Figure 39, from left to right: 327-333, 381-389, 437-444, 773-780, 847-853, 1163-1171.

The total volume above mean low water decreases when either the west or the east inlet is closed compared to when both are open (Figure 32). The shape of the graphs is almost identical but the ripples of the semi-diurnal tide are more pronounced when the east inlet is open.

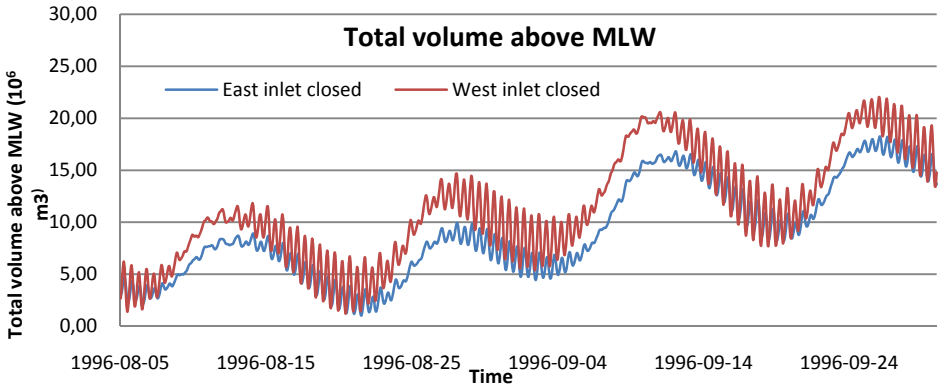

Figure 32: Total volume above local mean low water over time inside the lagoon when either east (Scenario 3) or west (Scenario 2) inlet is closed.

6.2.2 Tide-driven currents

During a tidal cycle water flows through the inlets in both directions. Since the tide is semi-diurnal at Bardawil Lagoon the water will enter and leave the lagoon twice a day. The amount of water that passes the inlets will depend on the size of the inlet and the current speed. Two observation points at each inlet were established in SMS in order to observe the velocity (Figure 33). Note that these observation points are different from the ones used to observe WSE.

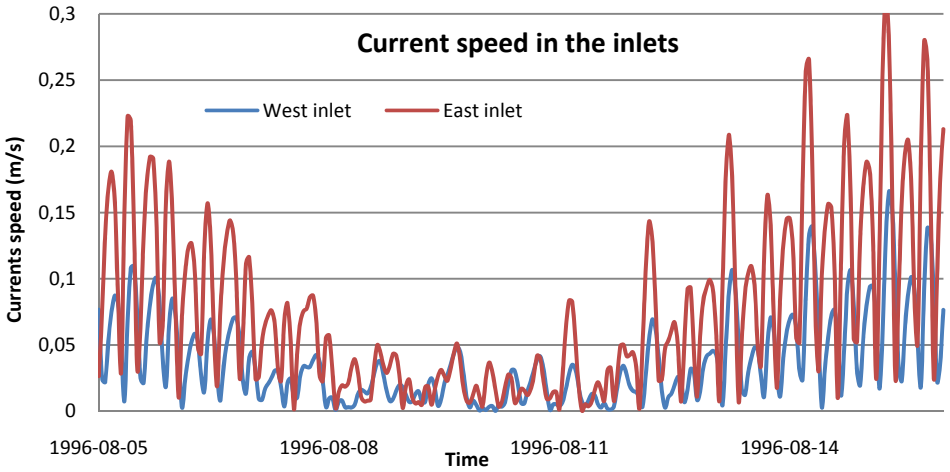

Figure 33: Current speed at two observation points in both inlets in mid August.

The velocity magnitude and direction pattern for outflow and inflow around the inlets are shown in Figure 34 and Figure 35 respectively. It is evident that flow through the east inlet influences a larger body of water inside the lagoon, independent of the flow direction. In all four pictures, the length scale is identical and the colour ramp scale ranges from 0 to 0.15 m/s, where red is zero and purple maximum.

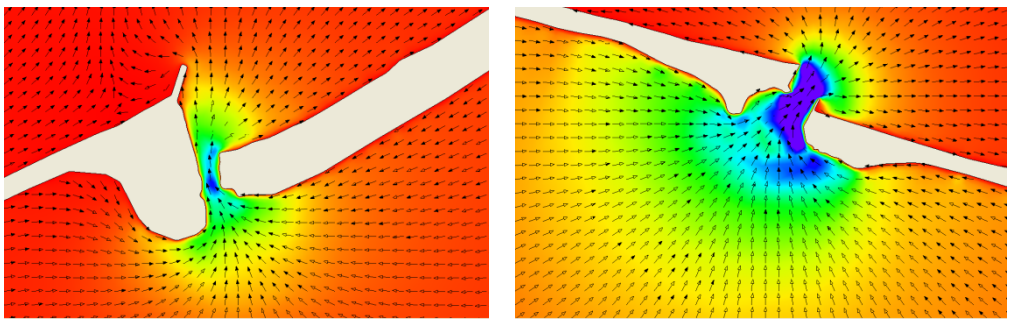

Figure 34: Outflow, its direction and magnitude, through west (left) and east (right) inlet for the same time step.

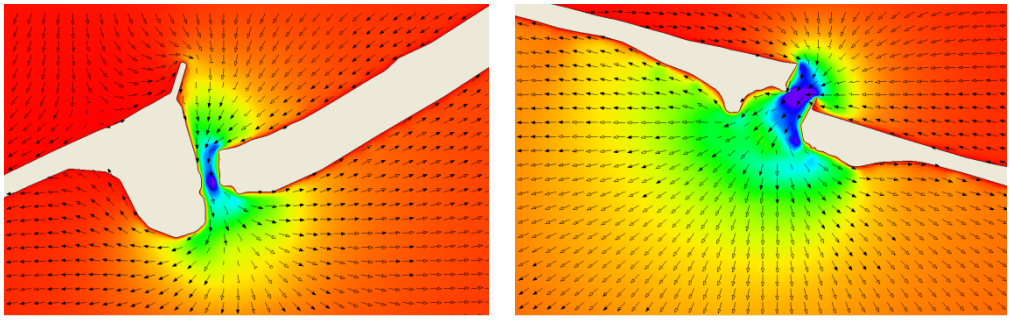

Figure 35: Inflow, its direction and magnitude, through west (left) and east (right) inlet for the same time step.

The current speed is constantly higher at the east inlet (Figure 33, Figure 34, and Figure 35). This is explained by both the larger changes in WSE at the east inlet compared to the west, Figure 30, and the direction of the tidal wave in Figure 36. The prevailing direction of the incoming tidal wave is almost straight into the east inlet, whereas it is perpendicular to the west inlet. These factors together with a slightly larger cross sectional area interact to induce a higher flow through the east inlet.

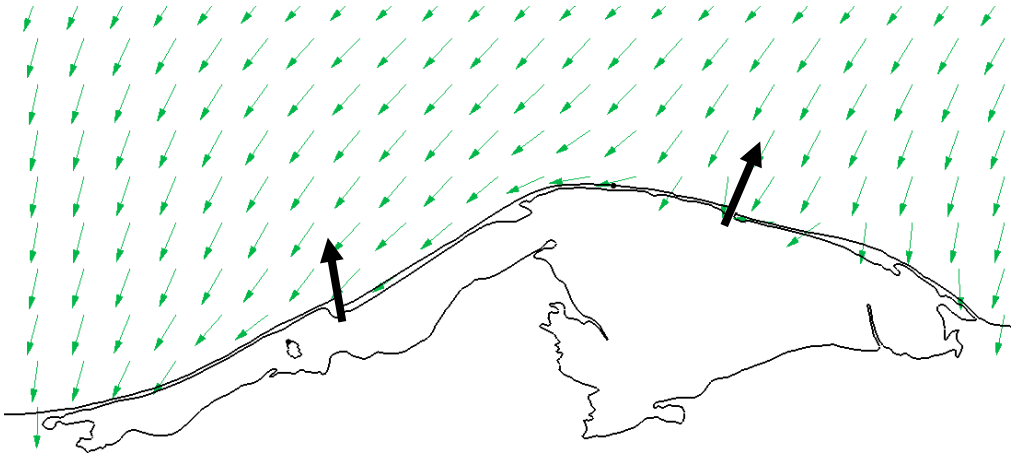

Figure 36: Prevailing direction of incoming tidal currents. Solid black arrows indicate entry direction of each inlet. Entry angle for west inlet is approximately 355 degrees and 18 degrees for east inlet relative north.

The cyclic pattern of the approaching and retreating offshore tidal wave is shown in Figure 37. There is little variability in the angle of approach, 40-80 degrees, and retreat, 270-340 degrees.

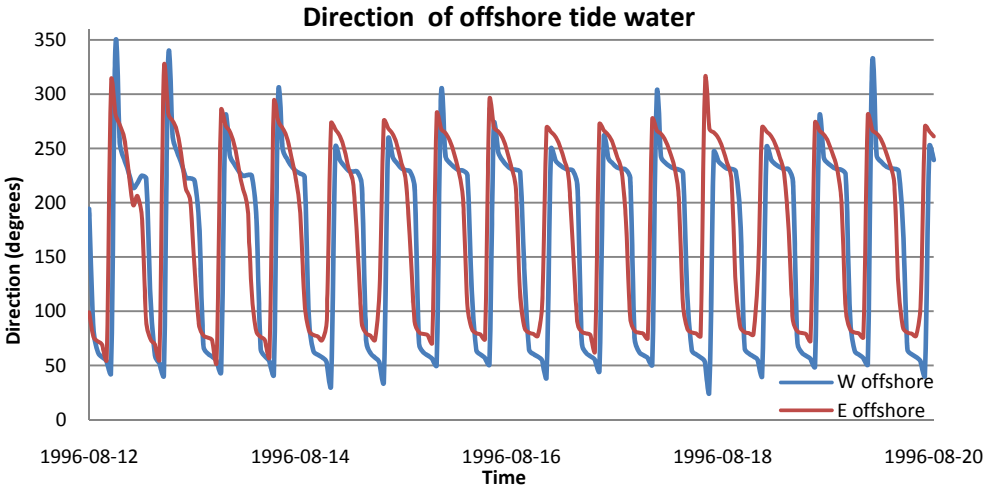

Figure 37: Predominant tidal water direction based on time series for 8 days in mid-August. Incoming tides at the offshore observation points approach the lagoon inlets with a direction ranging from 40-80 degrees. Outgoing tides retreat at approximately the incoming angle + 180 (270-340 degrees).

6.2.3 Net intertidal volume

This concept is of utmost importance in order to determine the overall exchange rate of the lagoon. The exchange rate is defined as the change in water volume inside the lagoon during a specific time, in this case roughly 12 hours, *i.e.*, a tidal cycle. In ADCIRC, the model sub-domain has been divided into 17 logical volumetric segments for measuring water surface elevations. Net intertidal volume is calculated as the difference between peaks and troughs in total volume above LMLW during a tidal cycle. Results for selected tidal prisms are shown in Figure 38 and Figure 39.

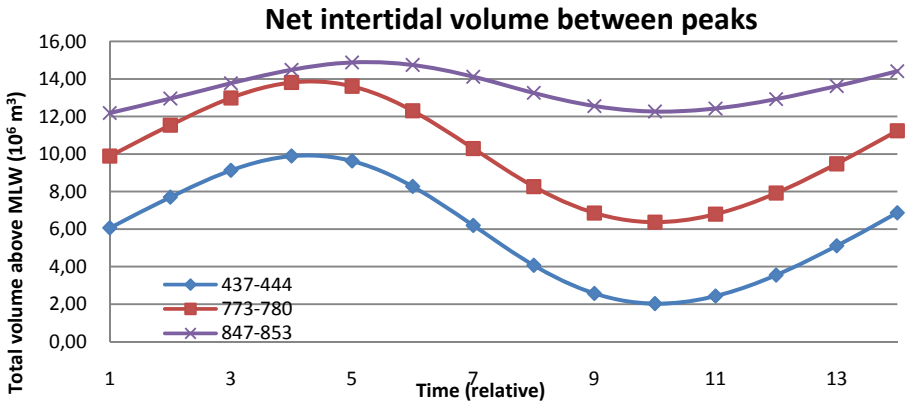

Figure 38: Plot of the total volume above MLW for each time step during a specific tidal prism. The net inter-tidal volume is found as the difference in volume between the maximum and the minimum of each curve. Three specific tidal prisms are shown in the graph (curve ID equals the time in hours from the start of the simulation), where the time between peaks and troughs vary slightly.

The graphs clearly show the variability in the net intertidal volume. In Figure 38 and Figure 39 the lagoon is draining and filling, respectively. The amplitude of the curves differs greatly which can be attributed to the large-scale variability of the tidal signal from the sea. For example, the prism 847-853 occurs at day 96-09-05 in the simulation which is right at the end of a semi-diurnal ripple, where the amplitude is low (Figure 31). Even though the net intertidal volume is low during this cycle, the total volume above MLW in the lagoon is quite high (ca. $13 \cdot 10^6$ m^3). During other intervals, such as 437-444, the total MLW is low, but the amplitude of the net intertidal volume is high. Analysis indicated (not shown in report) that there is no correlation between the total volume above MLW and net intertidal volumes. The time phase in between peaks and troughs is on average 6 hours, with minimum of 5 hours and maximum of 8 hours.

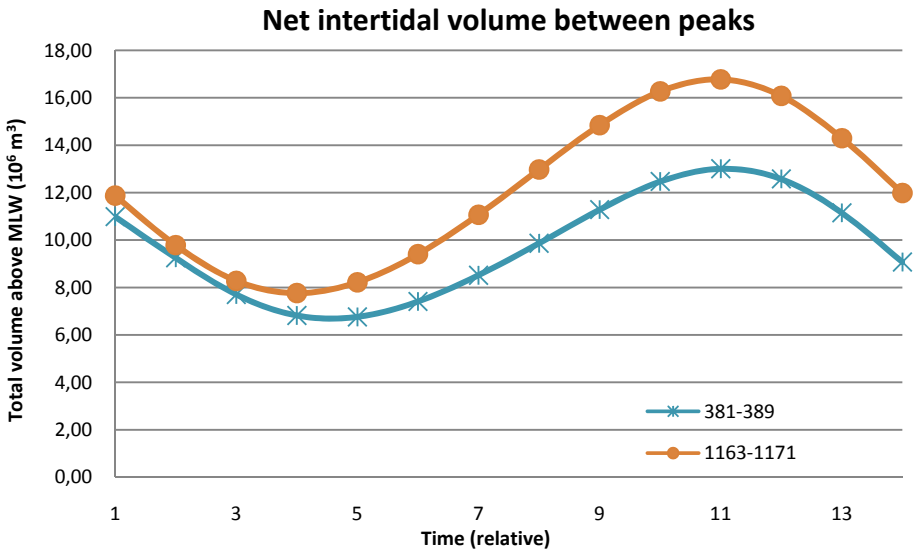

Figure 39: Plot of the total volume above MLW for each time step during a specific tidal prism. The net inter-tidal volume is found as the difference in volume between the maximum and the minimum of each curve. Three specific tidal prisms are shown in the graph (curve ID equals the time in hours from the start of the simulation), where the time between peaks and troughs vary slightly.

Larger timescale trends can be seen in Figure 39. Both curves start out at roughly the same minimum value of total volume above LMLW at hour 4/5, but due to differences in large-scale trends in the tidal water, the two tidal prisms reach their maxima on two quite different values. Curve 1163-1171 has a significantly higher peak value compared to 381-389.

To test Pritchard's method, the net intertidal volume is compared to the computed volume of water transported through the inlets at the same time tidal cycle. Plotting the volumes against each other in Figure 40 shows a strong correlation between the methods with a coefficient of 0.9983.

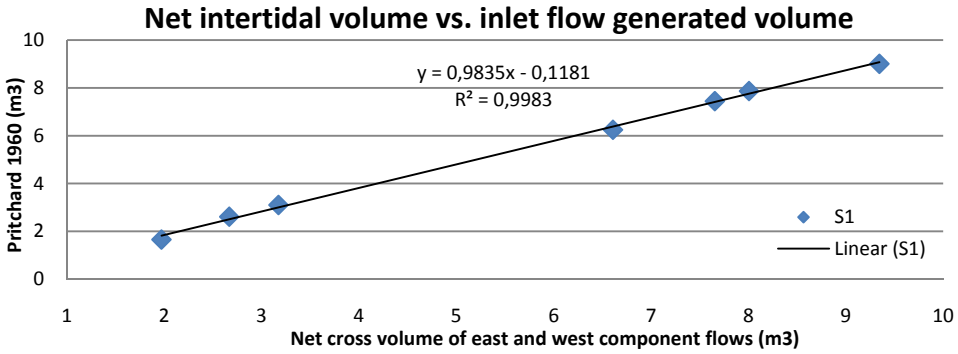

Figure 40: Scatter plot of net intertidal volume and the corresponding volume of water transported through both inlets for the same time period. Each point in the scatter represents a tidal prism (time interval).

Ideally, both methods should give the same result, however, there is a small systematic error that can be identified by either computing the volumetric difference (dV in Table 7) or the equation of the linear fit line in figure. The y-intersect is -0.1181 million cubic meters. The systematic error is attributed to the temporal differences of water surface elevations due to the progressive nature of the tide in the segments, *i.e.*, each segment may at times both include a positive and a negative water surface elevation change.

Table 7: Summary of volumes determined using Pritchard's net intertidal volume and measured volume across observation profiles at the inlets. The variable dV gives the difference between the methods. Exchange rate is determined according to Equation 12.

Tidal spectrum, time between maxima and minima (h)	Simulated volume in lagoon due to flow through inlets (10^6 m^3)	Net intertidal Volume (10^6 m^3)	dV (10^6 m^3)	Exchange rate per day
437-444	8.006	7.869	-0.137	0.023
773-780	7.655	7.446	-0.208	0.022
327-333	3.171	3.103	-0.068	0.009
847-853	2.666	2.612	-0.053	0.008
1163-1171	9.346	9.010	-0.336	0.026
888-900	1.969	1.66	-0.314	NA
381-389	6.608	6.25	-0.360	0.018

The exchange rate varies by a factor of two (from 0.9% to 2.3%) within the selected tidal periods, making it important to examine distribution of net intertidal volumes for a larger group of tidal prisms in order to accurately calculate a representative average.

To obtain a representative average, analysis has to be made on a section of net intertidal volumes in time that includes the majority of the phase and amplitude features inside the lagoon. The section selected (simulated day 26-35) contains the majority of the short-scale ripple seen in Figure 31 in between two periods of unidirectional flow (filling). In this time period, net intertidal volume has been determined for each 12-hour cycle. The result of the analysis is presented in Figure 41 and Table 8. Exactly the same period has been investigated for the two special scenarios, *i.e.*, east and west inlet closed. It should be noted from Table 8 that the

average value of the net intertidal volume for Scenario 3 (east closed) is approximately twice that of Scenario 2 (west closed).

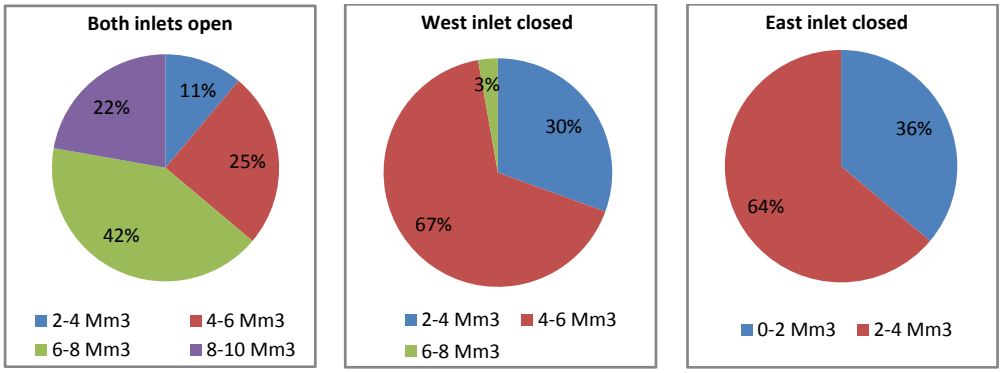

Figure 41: Distribution of net intertidal volumes for each tidal prism during simulated hours 631-847. Statistical data for the data set is show in the table.

Table 8: Statistical data for the set of net intertidal volumes presented in Figure 41.

Parameter	Both inlets (S1)	West closed (S2)	East closed (S3)
Average (10^6 m^3/tidal cycle)	6.40	4.39	2.12
Minimum (10^6 m^3/tidal cycle)	2.61	2.01	0.71
Maximum (10^6 m^3/ tidal cycle)	8.84	6.02	3.07
Exchange rate (day^{-1}) based on average (r_v)	0.0186	0.0127	0.00618

6.2.4 Renewal time

Renewal time refers to the process when water particles of different origins change places, due to tidal action only, with complete mixing occurring within the lagoon. The renewal times ($t_{50\%}$ and $t_{99\%}$) are determined on the basis of water particles originating from the Mediterranean Sea being exchanged with water particles originating from the lagoon. Salinity is not being taken into consideration, see section 6.4.2.

Table 9: Results from applying Equation 12 (Pritchard, 1960) & (Kjerfve, et al., 1996) to determine $t_{50\%}$ & $t_{99\%}$, which are the replacement times through mixing for half and 99% of the water, respectively.

Parameter	Both inlets open (S1)	West closed (S2)	East closed (S3)
$\Delta\overline{V_{net}}$ $(10^6\ m^3)$	6.40	4.39	2.12
$\Delta\overline{Q_{net}}$ $(10^6\ m^3/\text{day})$	12.8	8.78	4.24
$\overline{V}$ $(10^6\ m^3)$	689	691	687
$t_{50\%}\ (days)$	37.3	54.5	112
$t_{99\%}\ (days)$	248	362	746

By examining the results for the 50% renewal time for the different scenarios, it is evident that having two inlets open significantly reduces the renewal time. Closing the east inlet will have more adverse effects on the lagoon renewal time compared to closing the west. These results correlate well with earlier results in Figure 41 and Table 8.

6.3 CMS-Flow

In the simulations with ADCIRC the only input was the tidal changes in water surface elevation. However, the wind will also play an important role in the exchange of water through the inlets and in the internal water circulation of the lagoon (Miller, et al., 1990). To separate the effects of wind and tide three different scenario runs were performed in CMS-Flow using a run time of 12 days: Scenario 4 with wind data as the only input, Scenario 5 using WSE as the driving force only, and Scenario 6 including both WSE and wind.

6.3.1 Wind-driven circulation

The effect of the wind on the water surface elevation at the observation points is shown in Figure 42. The observation points are the same as for the ADCIRC simulations. The winds, mainly coming from NW and NNW during the specific run time, push the water inside the lagoon creating a larger setup inside the lagoon than at the inlets, since setup is fetch dependent.

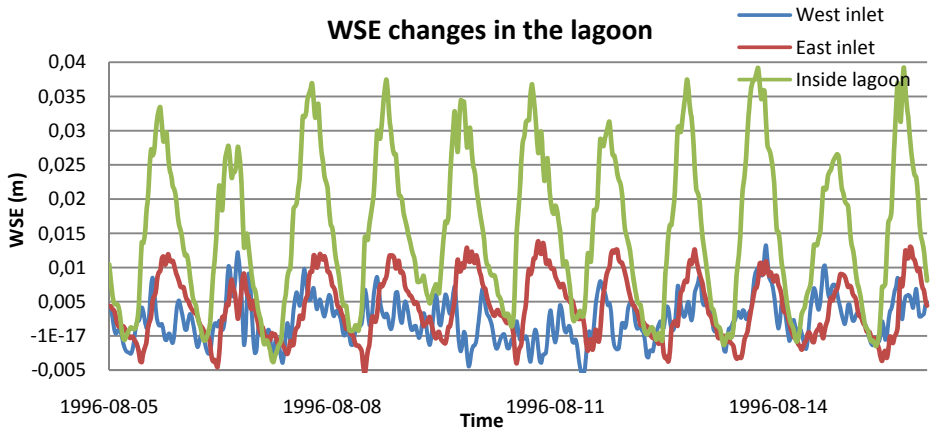

Figure 42: WSE (m) changes at three observation points with wind as the only input.

During each 24-hour wind cycle of strong daily winds and calm nightly conditions, the lagoon alters between two states. As wind speeds pick up in the morning, the blowing wind causes an increased surface stress on the water in the model domain. Once the forces due to the surface stress exceed the friction forces, setup occurs in the direction of the wind as well as setdown in the reverse direction. For the duration of the blowing wind, the water in the setup and setdown configuration are in non-equilibrium with each other. The time it takes to reach a state of equilibrium depends on the wind speed, direction, and fetch length. For Bardawil Lagoon, a state of equilibrium is never reached because the wind speed and direction continuously changes (a state of equilibrium would be represented by a horizontal line in Figure 42). At the onset of evening conditions, *i.e.*, subsiding winds and calm conditions, the surface stress due to wind dissipates and setup water propagates into areas of setdown due to gravity. The cyclic behaviour of the vertical dislocation of the water within the lagoon, at three observation points, can be seen in Figure 42.

The governing daytime force for the west inlet flow is the wind velocity (prevailing wind direction NW-NNW). The correlation can be seen clearly in Figure 43, both with regard to amplitude and phase. The most significant inward flow is generated by wind speeds exceeding 4 m/s, which are most frequent during the daytime. This type of flow can be characterized as wind-induced.

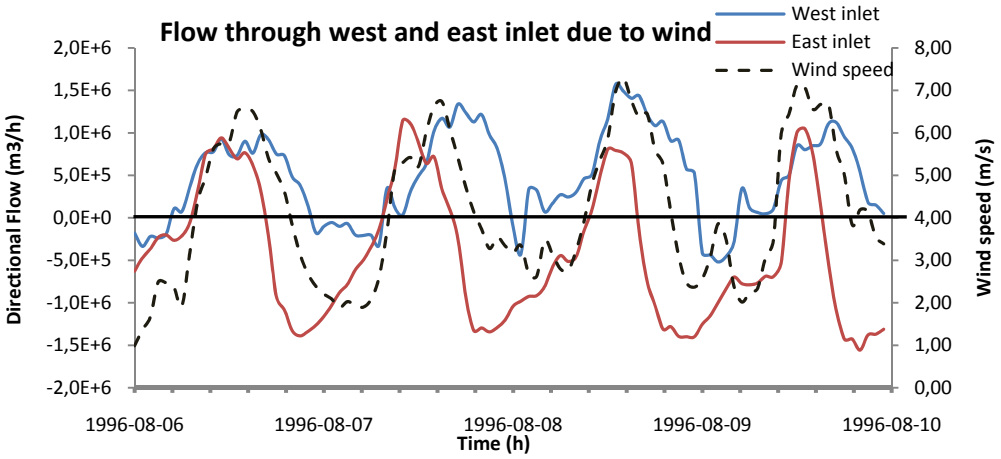

Figure 43: Flow through the western and eastern inlet in m3/h. Positive values indicate water flowing into the lagoon and negative values water flowing out of the lagoon. Wind speed from the NW-NNW direction for the same period is plotted on the secondary (right) y-axis.

During night, wind velocity progressively decreases, which affects the wind-induced flow. Inflow through the west inlet remains significant for a few hours after the wind dissipates, which can be attributed to residual water moment. This phase lag between the wind speed and positive flow through the western inlet can be seen in the figure. The eastern inlet behaves in a different manner, mainly due to the difference in the direction of the incoming wind and the orientation of the inlet (Figure 44). At mid-afternoon each day, the water surface of the lagoon has increased to such a degree that the gravity forces of water inside the lagoon exceeds the forces due to the wind stress at the east inlet, causing a gravity-induced outflow. Because the wind never completely ceases to blow and the orientation of the western inlet relative the incoming angle of the wind, wind stress will exert a force such that the western inlet seldom experiences outflow.

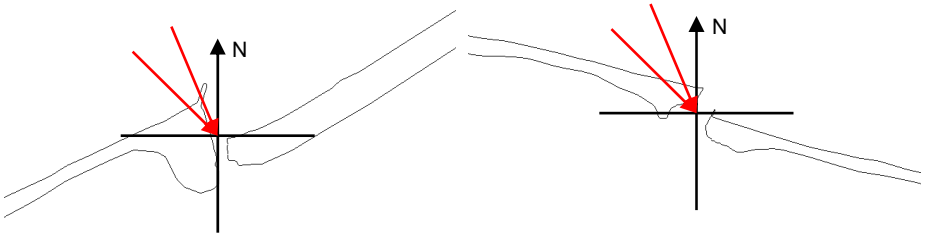

Figure 44: Orientation of the inlets relative to the prevailing wind direction. The orientation of the west (left figure) and east (right) inlet is roughly 355 and 18 degrees, respectively, with regard to N. Prevailing wind direction shown with red arrows (NW-NNW).

As stated in the previous section winds are strongest during the day, and taking the direction (NW to NNW) into consideration it is obvious that the wind pushes water into the lagoon. Once the wind speed subsides during the night the water that has entered during the day exits the lagoon. This results in two peak velocities during one day (Figure 45). The current speed due to wind exhibits a consistent pattern on a daily basis, but with substantial noise in the signal.

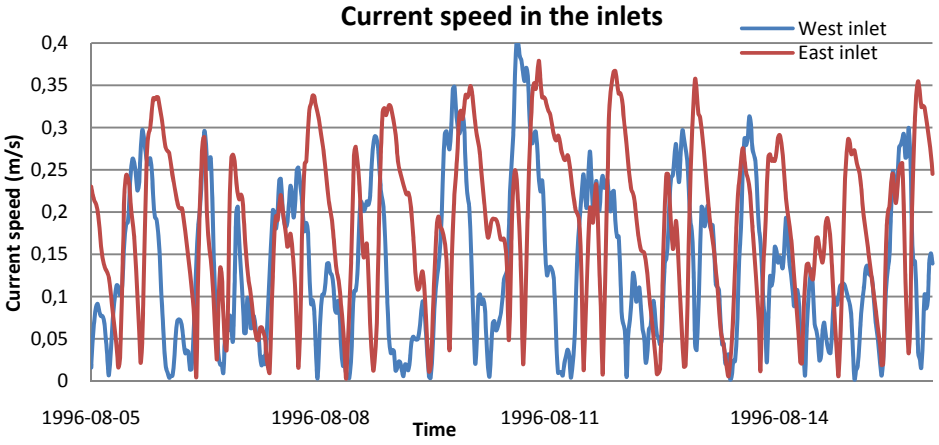

Figure 45: Current speed (m/s) at the inlets with wind as the only input.

6.3.2 Tide-driven circulation

In Scenario 5, with WSE as the only input, the current speed in the inlets reaches a magnitude of 0.9 m/s at the east inlet and 0.8 m/s in the west (Figure 46). The current speed varies with time following the semi-diurnal tidal motion giving rise to both high and low velocities. Comparing with the wind-induced currents (Figure 45) the speed is significantly higher due to the tidal action, but show a greater variation over time (Figure 46).

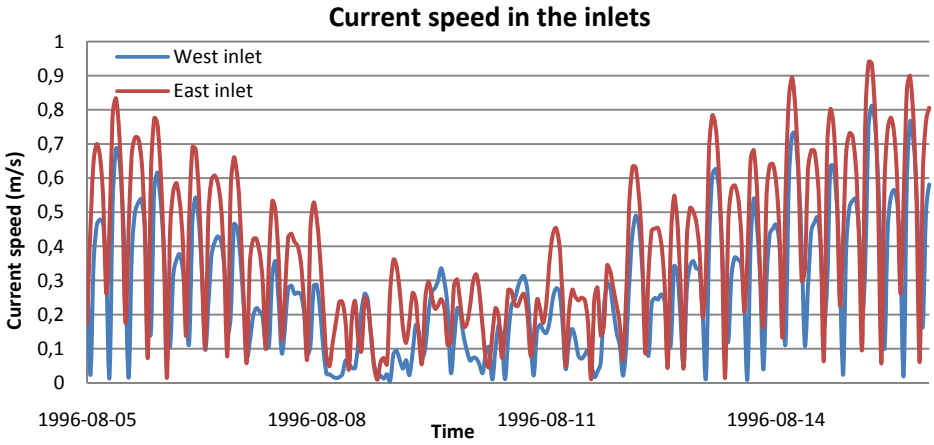

Figure 46: Current speed (m/s) at the inlets with tide as input.

6.3.3 Circulation from wind and tide

Using both wind and tide as input result in similar WSE changes at the inlets and inside the lagoon (Figure 47). The tidal changes will have a greater impact on the water surface elevation at the inlets, whereas the wind also affects the internal parts of the lagoon. The change is mainly positive at the observation point "inside lagoon" since the wind creates a setup and not a setdown due to the wind direction.

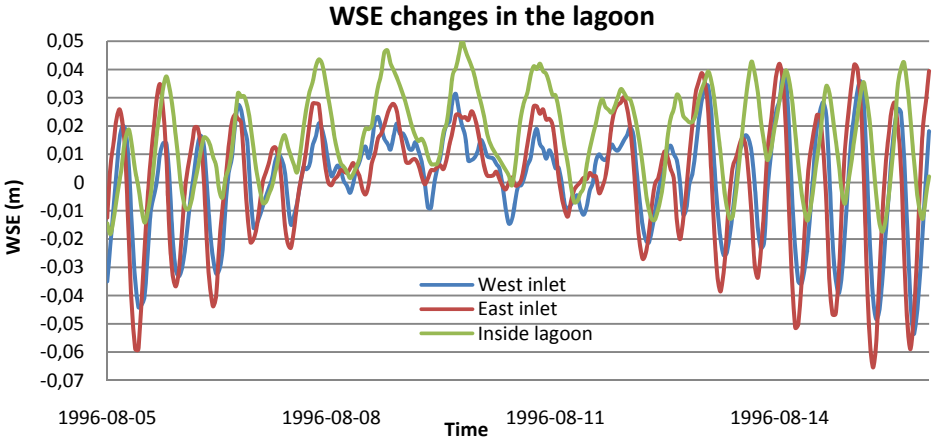

Figure 47: WSE (m) changes at three observation points with wind and tide as input.

The tide gives rise to a current speed maximum of 0.9 m/s (Figure 46) and the wind 0.4 m/s (Figure 45). When combining the wind and tide the maximum current speed is almost 1.0 m/s (Figure 48). This clearly shows that there is no additive effect between the wind and tide. To understand why, the detailed forcing pattern of the wind and the tide has to be investigated. Wind forcing behaves in a diurnal pattern with high wind speeds during the day (high surface stress and consequently high inlet currents) and the direction of the wind is more or less constant during the simulation, which means that wind forcing is mainly contributing to a net inflow of water at the west inlet and net outflow at the east (Figure 43). Tide on the other hand is of a semi-diurnal cyclic pattern that is responsible for equal inflow and outflow. Incorporated in the same model, the two modes of forcing are not in phase with each other and the wind can either reinforce or counteract the tidal currents.

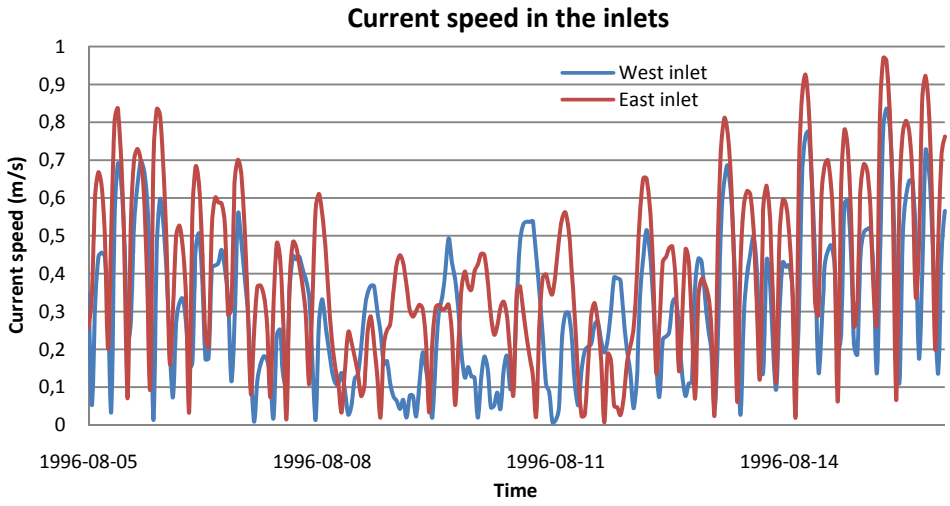

Figure 48: Current speed (m/s) at the inlets with wind and tide as input.

The reinforcing and dampening effect of the wind is illustrated in Figure 49 (west inlet) and Figure 50 (east inlet), where the current speed for Scenario 5 is plotted against Scenario 6. If there was no wind effect, the data points in Figure 49 and Figure 50 would follow the solid black line. However, this is not the case, and data points located above the line indicates a positive wind effect, wheras those located below indicates a negative effect. The wind effect, positive or negative, will be greatest when the tide-induced currents (Scenario 5) are weak. As a consequence of the even spread of data points below and above the black line the net wind effect on the flow through the inlets will be small.

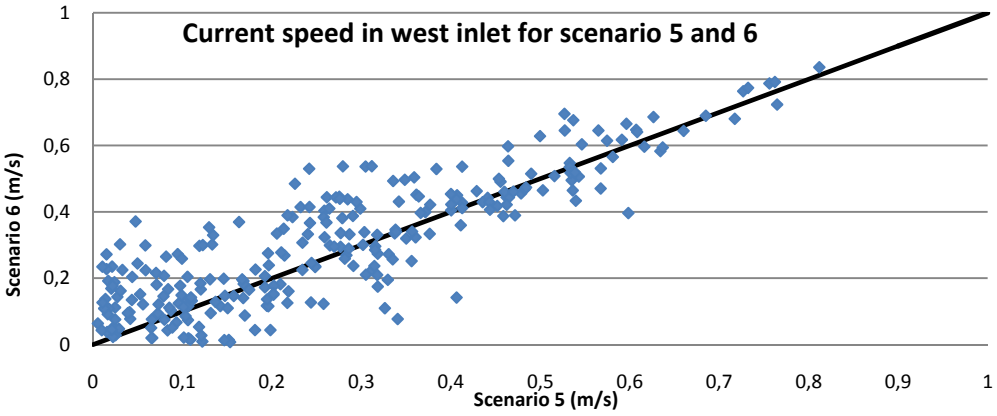

Figure 49: Current speed, in m/s, in the west inlet with Scenario 5 and 6 plotted on the x and y axis, respectively.

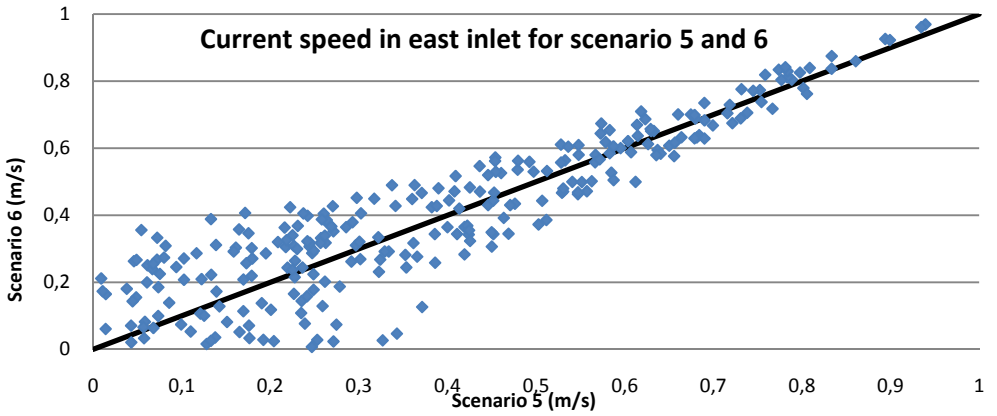

Figure 50: Current speed, in m/s, in the east inlet with Scenario 5 and 6 plotted on the x and y axis, respectively.

The velocity magnitude and direction pattern of outflow and inflow around the inlets are shown in Figure 51 and Figure 52, respectively. The pictures are taken when the currents are at a local maximum. It is evident that flow through the east inlet influences a larger body of water inside the lagoon, independent of the flow direction. In all four pictures, the length scale is identical and the colour ramp scale ranges from 0 to 0.20 m/s, where red is zero and blue maximum.

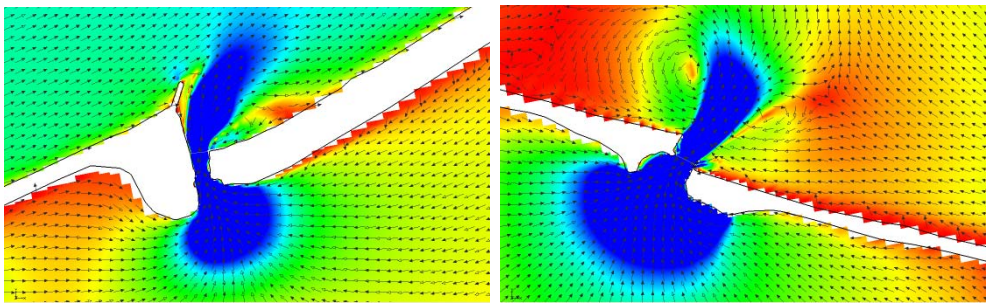

Figure 51: Outflow direction and magnitude through west (left) and east (right) inlet for the same time step.

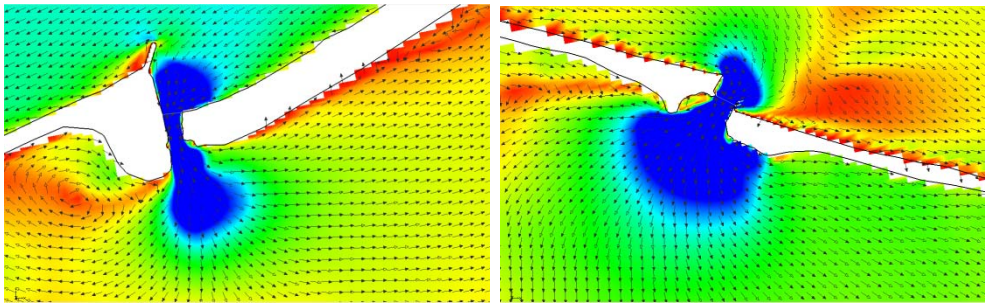

Figure 52: Inflow direction and magnitude through west (left) and east (right) inlet for the same time step.

Previously in the report, results consistently indicate higher flow through the east inlet independently of scenario. The relative importance of the inlets is shown in Figure 53. The ratio of the flow passing through each inlet is relatively constant but varies with scenario. For the tidal model (ADCIRC), the east inlet contributes to approximately 70% of the total flow. In Scenario 6, shown in Figure 53, wind together with tide alters the ratio of the total flow. The wind acts to level out the differences between the inlets and the contribution of the east inlet decreases to roughly 60%.

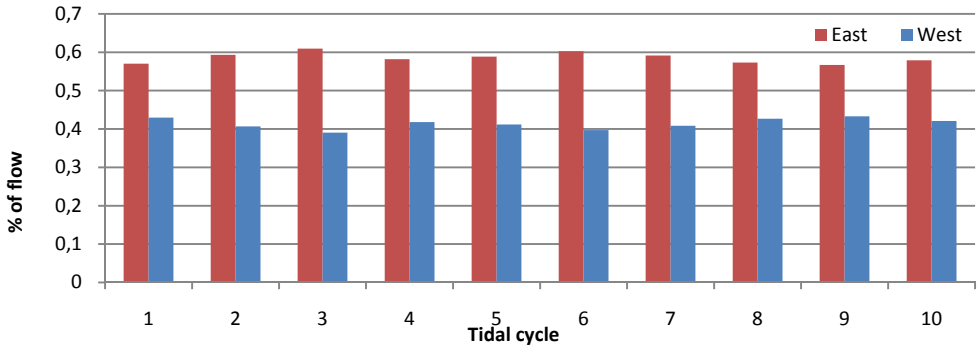

Figure 53: Accumulated volume per meter inlet presented as fraction of total volume.

6.3.4 Flow analysis

The correlation of flow through west and east inlet when the model is forced solely with tide action is very high, R^2=0.964, plotting the flow through the west inlet versus the east inlet. The results are expected considering the highly predictable and uniform nature of the tide.

The situation for the wind-driven model is quite different, which can be seen in Figure 54. The relationship between flows through the inlets appears to have a stochastic distribution and linear regression yields no significant correlation between the flows through the inlets (R^2 = 0.17). The magnitude of the flow and the direction depends on several factors, primarily wind speed and direction in relation to the orientation of the inlets, but also on the actual water level within the lagoon that may or may not cause a gravity-induced outflow (negative) through either inlet.

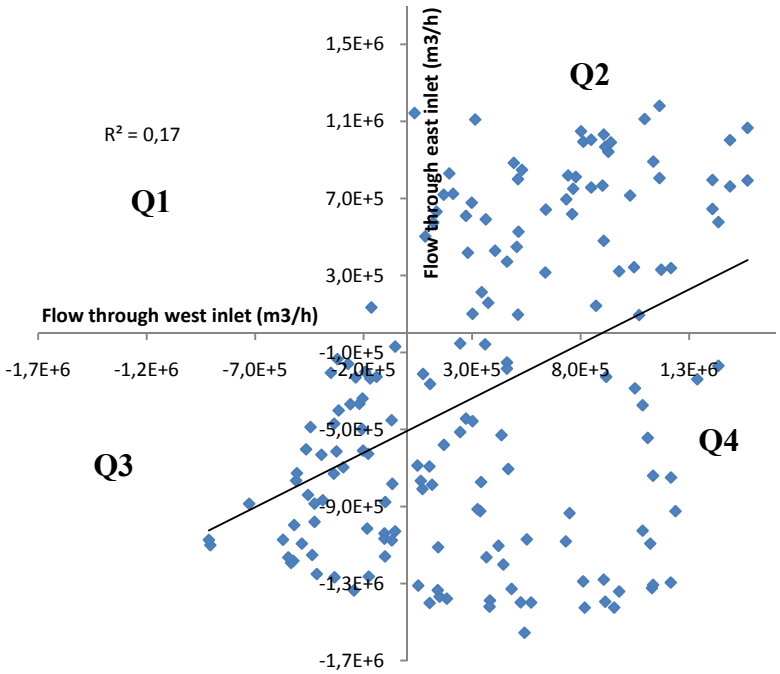

Figure 54: Flow, in m3/h, through the east and west inlet on the y and x axis, respectively, for Scenario 4 (wind only). Each quadrant (Qn) in the figure is numbered 1-4. Both axes have the same length and extend from ±1.7·10^6.

The plot summarizing the wind-driven scenario has been subdivided into four quadrants (Qn) for ease of interpretation. The quadrants represent the four possible flow outcomes:

Table 10: Possible flow directions through each inlet, where negative and positive flows are synonymous with outflow and inflow, respectively.

Inlet/Scenario	Q1	Q2	Q3	Q4
West	Out	In	Out	In
East	In	In	Out	Out

The most striking result is the absence of correlating points in Q1 which means that outflow through the western inlet and inflow through the eastern inlet never coincides. The rectangular shape distribution along the y-axis in Q3 indicate that whenever outflow simultaneously occurs the magnitude of the flow is significantly greater through the east compared to the west. In Q2 and Q4 the abundance and spatial distribution of data points is similar compared to each other. The shape of the distribution is square, or slightly rectangular, shaped and data is evenly distributed within the square, which suggests no correlation between direction and magnitude of flow through each inlet.

Once the circulation model is forced with both wind and tide the results change significantly compared to the previous case. In Figure 55 the results for the correlation plot of the model with tide and wind are shown.

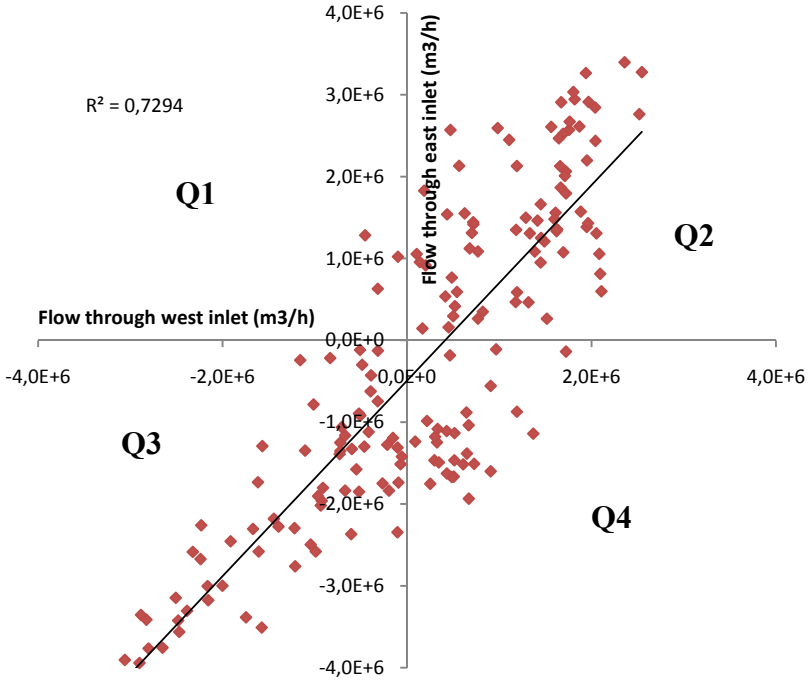

Figure 55: Flow, in m3/h, through the east and west inlet on the y and x axis, respectively, for Scenario 6 (wind and tidal action). Each quadrant (Qn) in the figure is numbered 1-4. Both axes have the same length and extend from ±4.0·10^6.

The stochastic behaviour of the wind-driven results is reduced when tide is added to the model. The correlation coefficient for Scenario 6 is $R^2 = 0.729$. On an imaginary scale with R^2 from tide only as the maximum value and R^2 from wind only as the minimum, Scenario 6 is an intermediate value more closely positioned to the maximum R^2. This suggests that tide is the determining factor for the flow direction at each inlet.

6.3.5 Internal circulation

In Figure 58 and Figure 59 internal circulation patterns and magnitude of flow is shown from parts of the actual CMS-Flow model (Scenario 6). The pictures are taken 5 hours apart to show the shifting behaviour of internal flow during one day. Tidal variations at the inlets and wind velocities for the selected day of the simulation are shown in Figure 56 and Figure 57.

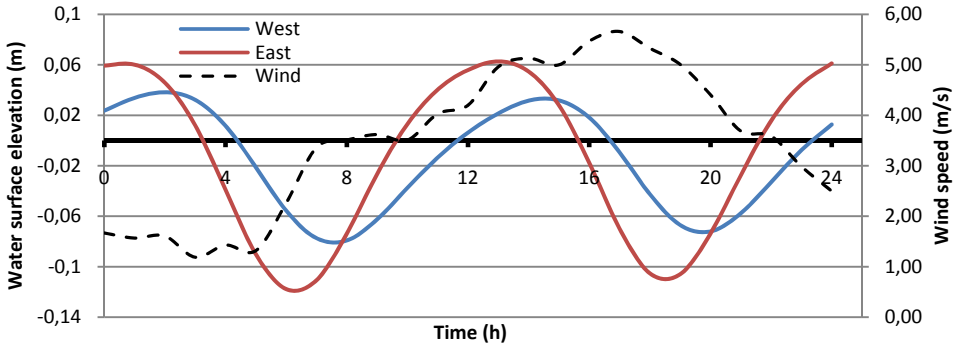

Figure 56: Tide forcing (water surface elevations) at the inlets.

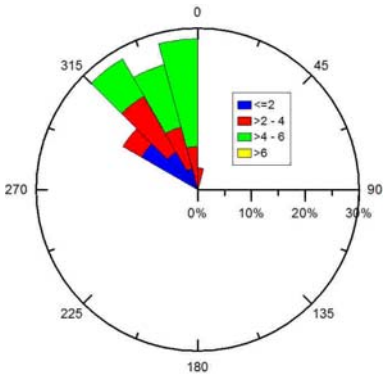

Figure 57: Wind forcing, speed (m/s) and direction.

Currents at both inlets in Figure 58 and Figure 59 are much stronger than in other areas within the lagoon at all times during the day. Note that the maximum value of currents is 0.20 m/s when in fact the actual speed is up to 0.70 m/s at the inlets. The direction of the currents alternates at several times mainly due to the tidal force. Areas in close proximity to the inlets experience direct effects of either ebb or flood. On the contrary, areas located further away are less affected by the changes at the inlets and more affected by wind. Along the western shore in Figure 59 currents occur during the afternoon due to the wind. The net effect of wind and tide in the eastern water body clearly show that mixing of water occurs. In the western arm (Figure 58) the water behaves as closed-basin flow, oscillating back and forth during the day in response to high and low water. Intermediate states do occur when tide is turning.

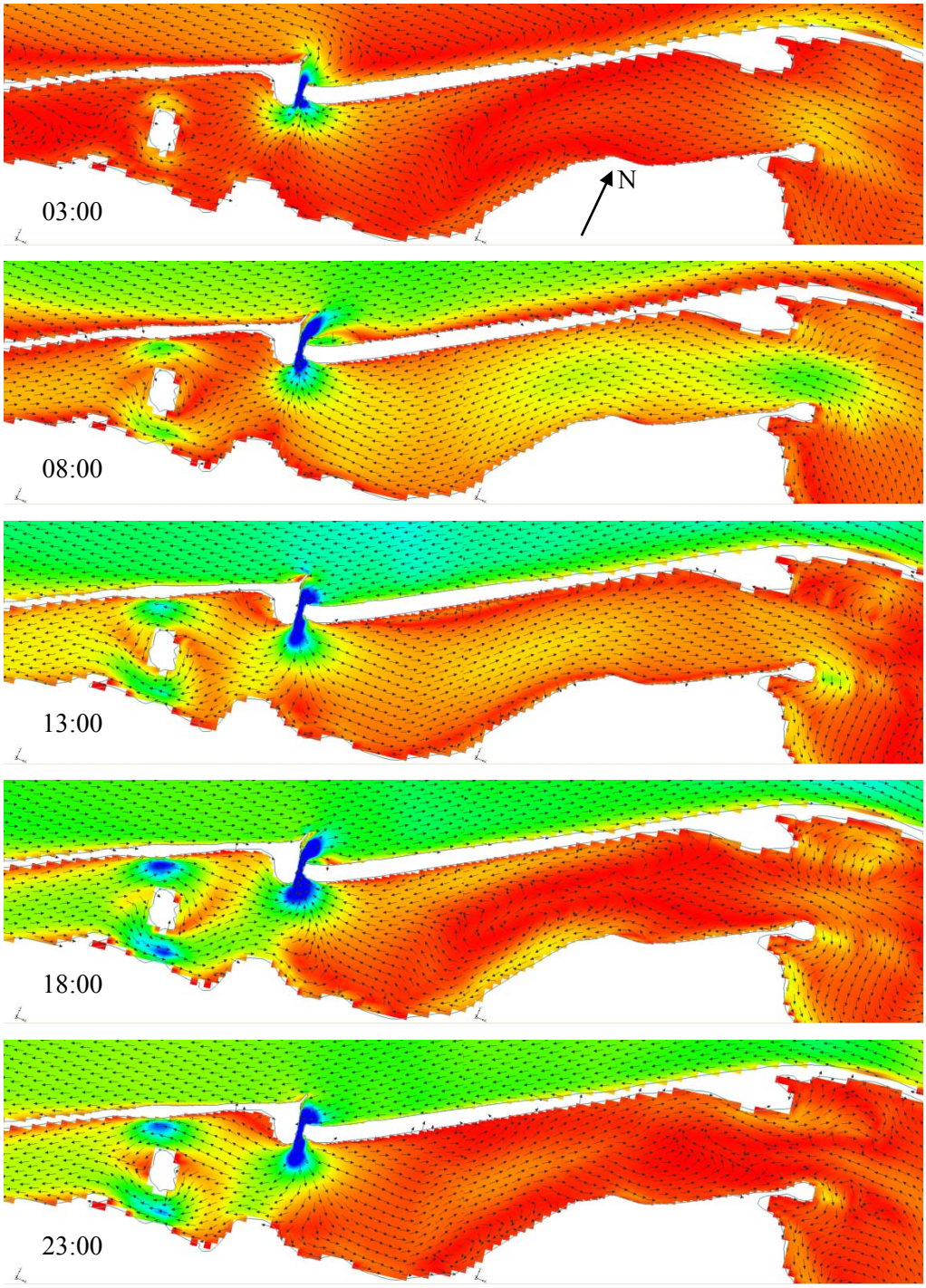

Figure 58: Internal circulation in the lagoon, from 03:00 to 23:00 during one day, of the western arm forced with both wind and tide in CMS-Flow. Colours show speed and arrows indicate direction.

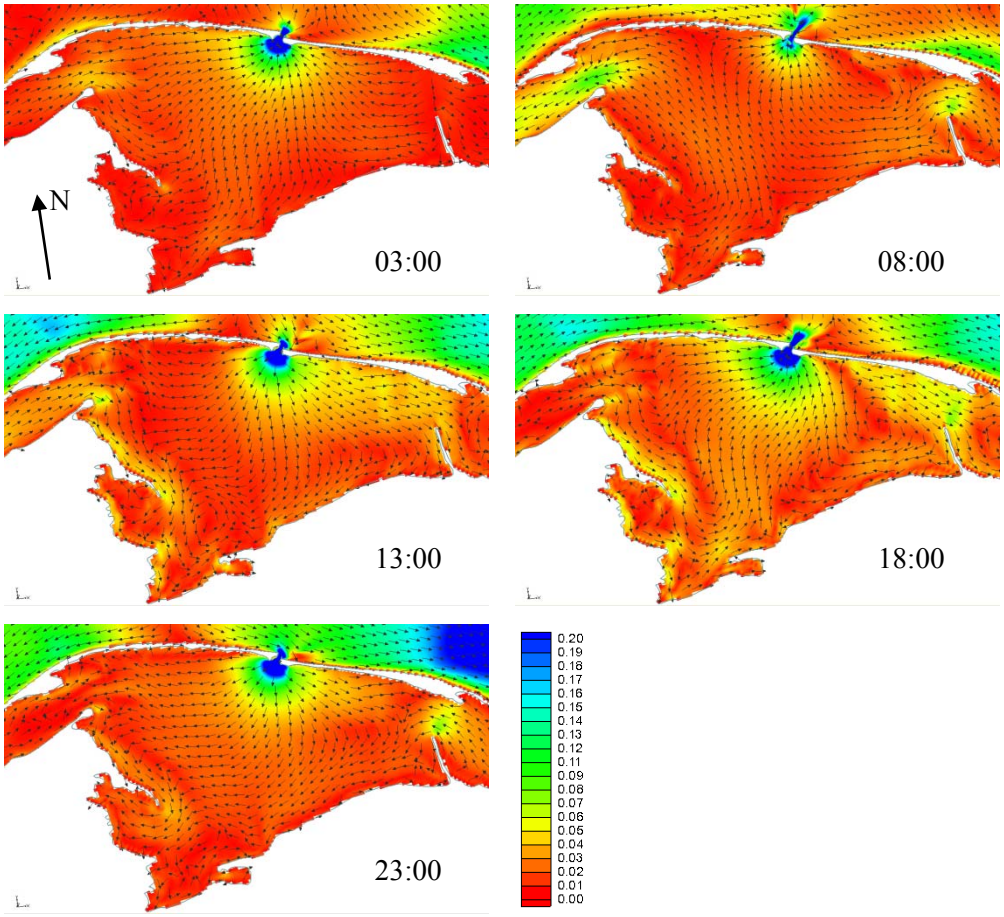

Figure 59: Internal circulation in the lagoon, from 03:00 to 23:00 during one day, of the eastern part forced with both wind and tide in CMS-Flow. Colours show speed and arrows indicate direction. The velocity magnitude legend is limited to 0.20 m/s.

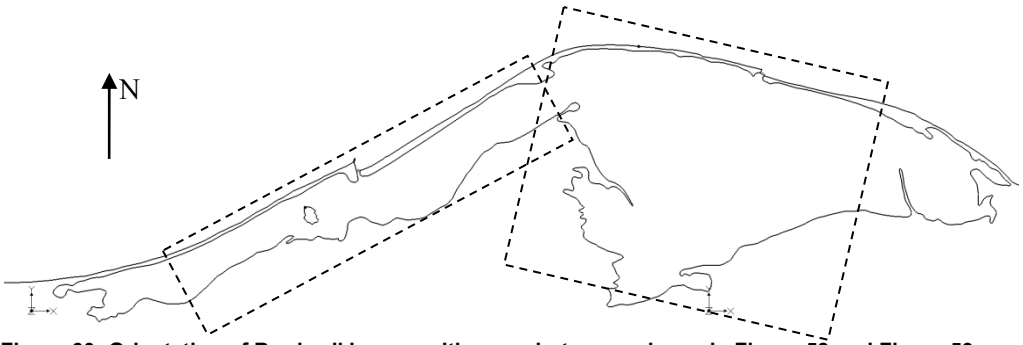

Figure 60: Orientation of Bardawil lagoon with snapshot areas shown in Figure 58 and Figure 59

6.3.1 Renewal time

Previously in the report, it has been established that the volume of water that passes through the inlets per day is equal to the net intertidal volume, hence the same method for determining the exchange rate and renewal time can be applied. In Table 11 the results from the Scenario 6 (WSE and wind forcing) clearly show that wind has a marginal effect on the renewal time. The 50% and 99% renewal times differ no more than 2%, which is the net wind effect.

Table 11: Comparing Scenario 5 and 6, 96-08-05 to 96-08-16.

Parameter:	WSE forcing (S5)	WSE & Wind forcing (S6)
$\Delta\overline{Q_{net}}$ ($10^6\ m^3$/day)	47.95	48.89
Exchange rate (r_v)	0.070	0.071
$t_{50\%}$	9.95	9.77
$t_{99\%}$	66.2	64.9

6.4 Post processing and calibration

ADCIRC and CMS-Flow simulations produced markedly different results when the same input was employed for default model parameter values. The current speed differs significantly and CMS-Flow yields up to 4 times higher values than ADCIRC, which leads to totally different flows and renewal times. The source of the differences lies in part with the fact that they are two different models with somewhat different approaches to model specific processes and to assign model parameter values. ADCIRC is a large-scale tidal model designed primarily to determine changes in water surface elevations, whereas CMS-Flow is a small-scale local inlet model with the primary purpose of calculating currents and flows in and around estuaries. Despite the model differences, the variation in the results is too great and an approach to reconcile the differences through a calibration procedure is needed. One important purpose of the present study is to estimate the renewal time of the lagoon; hence the model is calibrated with respect to the current speeds at the inlets. Since CMS-Flow is specially designed to model inlet velocities and has been validated through several studies with similar conditions, Scenario 5 is set as the calibration target for ADCIRC, *i.e.*, assuming that CMS results are closer to the actual currents at the inlets. Due to the lack of field data this is the best assumption possible at present. At shallow inlets, the determining factor for the water speed is mainly the friction coefficient C_f. ADCIRC was calibrated with respect to the friction coefficient, which was done by means of trial and error to obtain current speeds in ADCIRC that more closely matched the target velocities obtained with CMS-Flow. During the calibration simulations in ADCIRC it was found that the model has a lower limit for the linear friction coefficient. At C_f = 0.0004 the model is unstable and is unable to calculate a solution. The best inter-model fit was obtained using C_f = 0.0008. Model correlation between the CMS and ADCIRC simulations, R^2, was 0.614 for the west inlet (Figure 61) and 0.715 for the east inlet (Figure 62). The correlation is neither better nor worse by comparing to the correlation between the target model and ADCIRC using 0.0025 for friction coefficient. The lack of greater correlation is most likely due to fundamental differences in the two models and the fact that only one parameter is calibrated for.

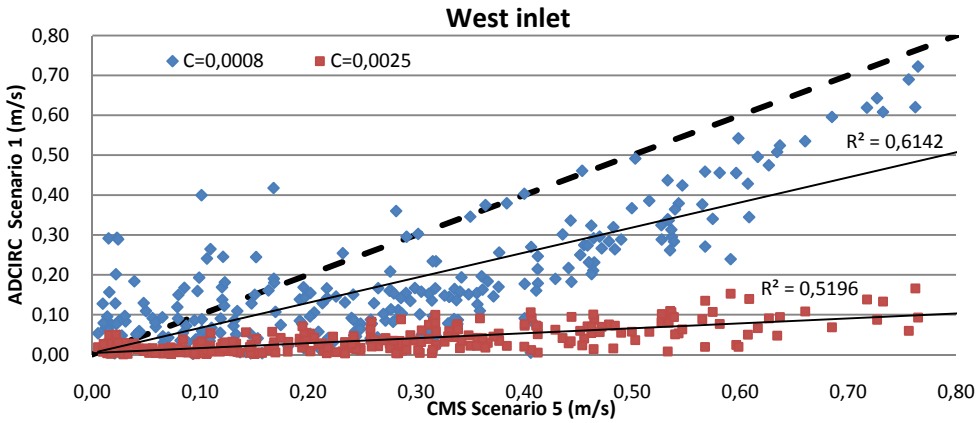

Figure 61: Calibration results for the west inlet showing initial ADCIRC model with friction coefficient of 0.0025 and best fit with 0.0008. Target model, *i.e.*, CMS Scenario 5 is plotted on the x-axis and ADCIRC on the y-axis. The dashed line indicates the optimal calibration.

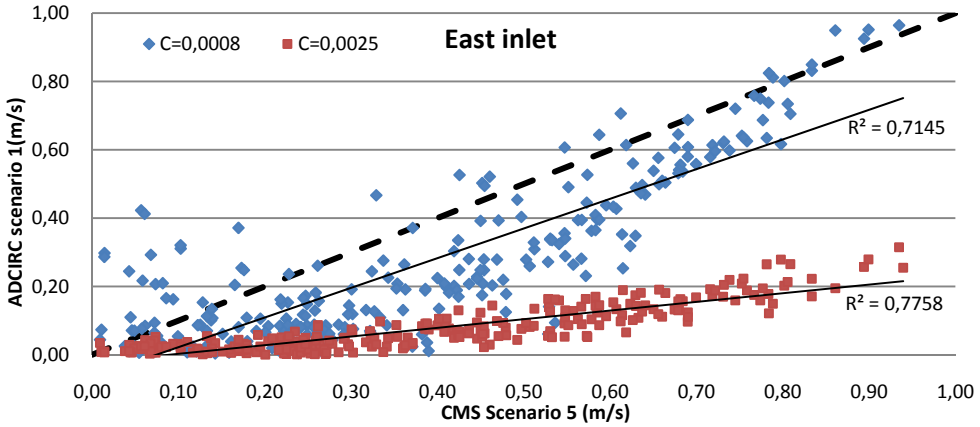

Figure 62: Calibration results for the east inlet showing initial ADCIRC model with friction coefficient of 0.0025 and best fit with 0.0008. Target model, *i.e.*, CMS Scenario 5 is plotted on the x-axis and ADCIRC on the y-axis. The dashed line indicates the optimal calibration.

The aim of the calibration was to increase the inlet velocities of the ADCIRC model such that they more closely represent the velocities calculated by CMS in Scenario 5. The dashed line represents optimal calibration. It is clear from the figures that Scenario 1 using 0.0008 matches more closely inlet currents compared to 0.0025, *i.e.*, the gap between the linear regression line and the dashed target line is smaller.

ADCIRC results previously calculated in the report are based on the model using friction coefficient of 0.0025. The process of rerunning Scenario 1-3 and redo the data extraction and analysis is a highly time-consuming task. Therefore the scalability of the initial ADCIRC results with respect to the friction coefficient was tested. To do this, current speeds through each inlet were plotted (Figure 63) for C_f = 0.0025 against current speeds for C_f = 0.0008.

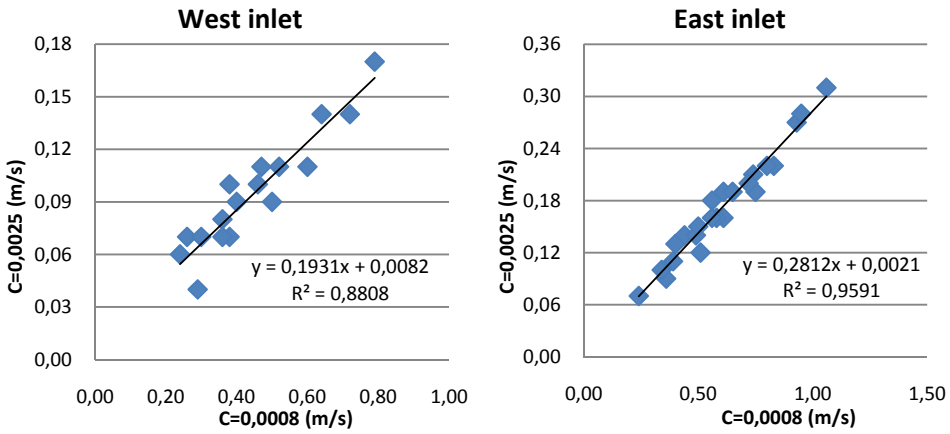

Figure 63: Current speed in m/s for two different simulations of Scenario 1 using different linear friction coefficients. Simulation using C_f = 0.008 and 0.0025 on the x and the y-axis, respectively.

From the graphs it is evident that the correlation of inlet currents between the different friction coefficient runs using Scenario 1 is good. This implies that the results in fact are linearly scalable. The equations of the linear regression lines for the west and east inlet have different slopes, which suggest that current speeds at each inlet must be corrected using two different scaling factors, f_w and f_e for west and east inlet, respectively. By comparing peak velocities during each tidal cycle during 12 days for both simulations the factor could be determined. For the west inlet, $\bar{f}_w$ = 4.80 and $\bar{f}_e$ = 3.53 for the east inlet.

In order to apply the scaling factors to the net intertidal volumes, a secondary inlet-independent factor f_{net} is required. In Figure 40, section 6.2.3, a clear relationship between the net intertidal volume and the volume of water resulting from measured flow through the inlets for seven tidal cycles was established. By applying the inlet-specific factor to the computed volumes due to flow it is possible to determine an inlet-independent factor by comparing the flows per tidal cycle to the original net intertidal volumes for the same tidal cycle. The cycle averaged inlet-independent scaling factor was $\bar{f}_{net}$ = 3.94, $\bar{f}_{net}$ can successfully be applied to the extended record of measured net intertidal volumes calculated for the 200 hour section to obtain friction-coefficient corrected volumes. These results are presented in the following section.

CMS-Flow simulations contain ADCIRC WSE results using C_f = 0.0025 as in data on the ocean boundary. The effects of an overestimated friction coefficient on the water surface elevations in the offshore region are small, since the forcing in CMS simulations is added in areas with a substantial depth, *i.e.*, the water particles are not affected by the bottom. Hence the CMS simulations required no correction.

6.4.1 Calibrated results

The scaling factors, f_w, f_e, and f_{net}, calculated in the previous section were applied to yield calibrated flow data from the inlets. These data were used to calculate new

exchange rates and renewal times for all three ADCIRC scenarios (Table 12). Results presented in Table 12 originate from the analysis of flows and net-intertidal volumes during the 200 h interval; see section 6.2.3, Table 8.

Table 12: Calibrated renewal times for Scenario 1-3 for the 60 day simulation (200h of data examined).

Parameter	Both inlets open (S1)	West closed (S2)	East closed (S3)
f	3.94	3.53	4.80
$\Delta\overline{Q_{net}}$ $(10^6\ m^3/\text{day})$	50.4	31.0	20.4
Exchange rate (r_v)	0.073	0.045	0.030
$t_{50\%}\ (days)$	9.48	15.4	23.4
$t_{99\%}\ (days)$	63.0	103	155

The results in Table 12 show an increase in the exchange rate for all scenarios. The increase is identical with the different scaling factors calculated previously due to the fact that all calculations are linear.

In the CMS simulations the run time is five times shorter (12 days compared to 60 days in ADCIRC) giving less representative exchange rates. Corrected renewal times for Scenario 1 were calculated for the corresponding run time in CMS to be able to make an accurate comparison between the models and scenarios (Table 13).

Table 13: Calibrated renewal times for ADCIRC Scenario 1 in comparison with CMS-Flow Scenario 5 and 6 (12 day simulation length).

Parameter:	ADCIRC WSE forcing (S1)	CMS WSE forcing (S5)	CMS WSE & Wind (S6)
$\Delta\overline{Q_{net}}$ $(10^6\ m^3/\text{day})$	39.8	48.0	48.9
Exchange rate (r_v)	0.058	0.070	0.071
$t_{50\%}\ (days)$	12.0	9.95	9.77
$t_{99\%}\ (days)$	79.8	66.2	64.9

Scenario 1 yields a longer renewal time compared to Scenario 5 and 6, which is expected since the corrected currents in Figure 61 and Figure 62 consistently are lower than those calculated in Scenario 5.

When calculating the renewal times for the lagoon, the residual flow due to evaporation and precipitation is not considered. Combining the lagoon residual flow, Q_f, and the net intertidal volumes would yield a better approximation of the renewal time. This is done by adding Q_f to $\Delta\overline{Q_{net}}$ and recalculating the renewal time using the new r_v values.

Table 14: Summation of lagoon hydraulic-flushing flow and net intertidal volume and the corresponding renewal time, $t_{50\%}$ and $t_{99\%}$ (60 day simulation length).

Parameter	Both inlets open (S1)	West closed (S2)	East closed (S3)
$\Delta\overline{Q_{net}} + Q_f\ (10^6\ m^3/\text{day})$	53.0	33.6	23.0
Exchange rate (r_v)	0.077	0.049	0.033
$t_{50\%}\ (days)$	9.01	14.2	20.8
$t_{99\%}\ (days)$	59.9	94.4	138

Adding the residual flow has a marginal effect, approximately 5% for Scenario 1, on the renewal times. The largest effect is observed when adding to Scenario 3 for which the east inlet is closed.

6.4.2 Renewal time using saline tracer

By theoretically tagging the particles, in this case salt, it is possible to determine the fraction of new particles entering the lagoon at each tidal cycle. This is a direct measure of the renewal time of water (Pritchard, 1960). The water flowing through the inlets during a flood contains both "new" water particles from the Mediterranean Sea as well as "old" particles that exited the lagoon during the previous ebb.

Measurements of the salinity levels in the lagoon were taken at two times, in July 1970 and in March 1973. At the first occasion the east inlet, Boghaz 2 in Figure 64, was closed. The inlet was artificially opened by dredging during the following years. In 1973, both inlets were open (Klein, 1986).

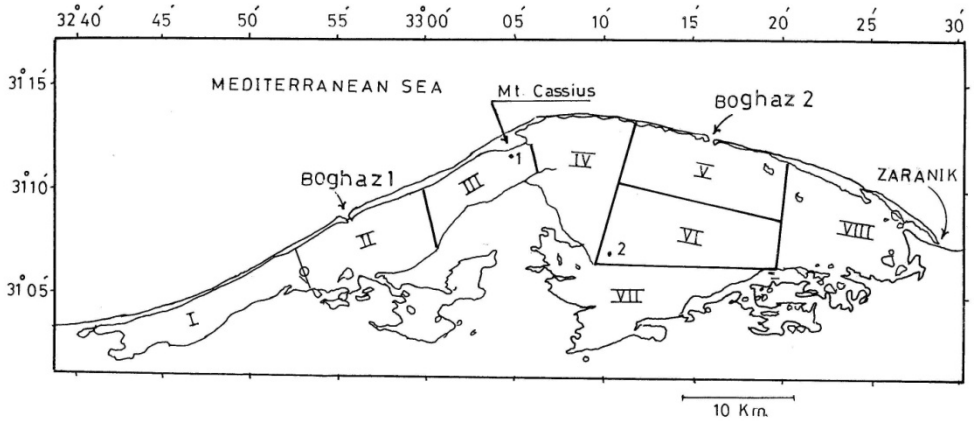

Figure 64: Map showing different zones for salinity measurements (Fanos, et al., 1994).

Due to lack of more recent data, these measurements will represent two of our scenarios, *i.e.*, July 1970 equals Scenario 3 (east inlet closed) and March 1973 represents the standard Scenario when both inlets are open. This is a practical simplification as well as an assumption that the inlet geometry from 1970 and 1973 approximately equals that of 1996.

The average salinity of the Mediterranean sea, s_{in}, is 39.2‰ (Fanos, et al., 1994). To determine n from Equation 16, the average salinity of the lagoon, $\bar{s}$, is determined from Table 15 for both years. The salinity of the out flowing water, s_{out}, is equal to the salinity in zone I at 1970, and calculated as the average between zone I and V in 1973 when both inlets were open. A summary of salinity data and calculated values of n is displayed in Table 16.

Table 15: Measured salinity at different zones in Figure 64. Zone I and VIII are estimated based on the level in adjacent zones. In July 1970, only Boghaz 1 was open, and Boghaz 2 was opened in 1971. The data from March 1973 is the most recent data available in which both inlets are open (Fanos, et al., 1994).

Zone	Salinity March 1973 (‰) Both inlets (S1)	Salinity July 1970 (‰) East inlet closed (S3)
I	48	70
II	41	60
III	43	70
IV	48	77
V	44	83
VI	52	90
VII	50	86
VIII	50	85

Table 16: Summary of salinities and results from Table 15 and Equation 16.

Parameter	Both inlets (S1)	East inlet closed (S3)
$\bar{s}$	47.0‰	77.6‰
s_{in}	39.2‰	39.2‰
s_{out}	42.5‰	60.0‰
n	0.423	0.542
$1/n$	2.36	1.85

Applying the results from Table 16 in Equation 17, while assuming that the change in salinity over time (ds/dt) remains zero, the outflow as fraction of the volume of the lagoon, T_{out}, can be determined. Using the corrected exchange rates, the ratio of new water, r_n, can be determined using Equation 18. The renewal time with respect to salinity (Table 17), assuming incomplete mixing, can be determined as the fraction of completely mixed renewal time, previously determined, and divided by the ratio of "new water".

Table 17: Determination of the fraction of "new water" and the resulting renewal time as defined by Pritchard (1960) using Equation 17.

Parameter	Both inlets (S1)	East inlet closed (S3)
$T_R\ (day^{-1})$	-0.00376	-0.00376
$T_{out}\ (day^{-1})$	0.0504	0.00800
Exchange rate (r_v)	0.077	0.033
New water (r_n)	0.65	0.24
$t_{50\%}\ (days)$	13.9	86.7
$t_{99\%}\ (days)$	92.2	575

Mathematically, r_n, is described as a function dependent on the residual flow, salinity gradients, and exchange ratio. Residual flow is independent of the total cross sectional area of the inlets, whereas enrichment of salt is a slow process and is directly dependent on the overall water exchange between the lagoon and the sea. In the case of Bardawil Lagoon, the climate is arid leading to loss of water to the atmosphere while salt remains. In order to obtain a representative value for the non-idealized case, lagoon salinity concentrations have to reach equilibrium prior to determining these values.

Results show that the renewal time increases by roughly 50% for Scenario 1 when incomplete mixing occurs (Table 17). Previously established renewal times are more idealized as they assume complete mixing. In the study of Chincoteague Bay by Pritchard (1960), the ratio of new water was found to be 34% (compared to 65% for Bardawil Lagoon) and the result was consistent with visual observations at the inlets. Although differences, *e.g.*, salinity of bay/lagoon, total volume, and inlet size, exist between the two lagoons, the order of magnitude of r_n found for Bardawil Lagoon matches that of Chincoteague Bay, which indicates that the results have some relevance despite lack of visual observation for comparison.

In the simulation where the east inlet is closed, the ratio of new water decreases drastically (24%). This scenario is based on salinity levels measured in 1970 (Coastal Research Institute, 1971-1999) and the results clearly show the dependency of "ratio of new water" to salinity gradients, which are substantially higher for Scenario 3 (Table 15).

7 Conclusion

Bardawil Lagoon has experienced different states in the past with regard to its connection to the Mediterranean Sea and the associated water exchange. Its current state is dependent on interventions by man to keep it open and ensure the water exchange with the sea. Longshore sediment transport tends to cause closure of the inlets, which affects the water quality of the lagoon. In a first detrimental step salinity levels increase, but eventually the lagoon completely dries up, if closure of the inlets occur. To properly manage the inlets (*e.g.*, optimize dredging to keep them open) and guarantee satisfactory water-quality conditions in the lagoon, detailed knowledge of the water exchange between the lagoon and the sea, as well as the internal circulation in the lagoon, is needed.

The main objectives of this study were to quantify the water exchange between the lagoon and the sea, and to determine the main physical factors controlling it. Also, the internal circulation of the lagoon was of interest and how various factors influence it. Predictive computer models were employed to estimate the effects of tide and wind on the renewal time of the lagoon and its internal circulation in order to determine the importance of the water exchange with the Mediterranean Sea for the lagoon water quality.

The eastern inlet is slightly larger than the western inlet, but this does not completely explain the higher flow through the east inlet. The incoming angle of the tidal wave and the larger WSE changes at the eastern inlet adds to the explanation. When only tide is considered the east inlet contributes to 70% of the total inflow and outflow. The wind diminishes the differences with approximately 10% and can have a reinforcing or dampening effect on the flow depending on the wind speed and direction. However, the tide is the main governing force for the direction and magnitude of the flow through the inlets.

The tidal effect within the lagoon attenuates with the distance from the inlets. Inside the lagoon wind governs the circulation and creates wind setup and setdown. Wind speed, duration, and fetch length decide the magnitude of wind setup.

Model results clearly show that it is advantageous for the renewal time with a larger inlet cross-sectional area. Simulations with either inlet closed directly affect the renewal time with a factor 1.5^{-1} or greater compared to the standard state. Assuming complete mixing, the 50% renewal time for the standard state was found to be 10-12 days with tide as the sole model forcing for 12-day simulation of CMS and ADCIRC, respectively. Adding wind to the model shows that the effects of tide and wind are not additive, and the renewal time is marginally shorter, 9.8 days. Long-term effects due to evaporation and precipitation are responsible for a residual inflow of $2.6 \cdot 10^6$ m^3/day. Calibrated and corrected (added residual flow) results for the 60-day ADCIRC simulations contain a larger data set and are therefore more reliable. The renewal time for the standard state model was determined to 9.0 days. No previous studies have estimated the renewal time, which explains the lack of comparative

values. Therefore can the quantitative performance of the model not be properly assessed.

The marginal effect of the residual flow increases in scenarios which have either inlet closed. Residual flow is dependent on evaporation and precipitation, but is independent on the total cross sectional area of the inlet. In simulations, the residual flow described as a ratio of the total flow is 7% when both inlets are open, while it increases to 47% when the east inlet is closed.

Moreover the renewal time was found to be closely dependent on salinity gradients. Using salinity as a particle tracer, assuming incomplete mixing, it was calculated that the fraction of new water that passes through the inlets during each tidal cycle was 65% for the standard state.

The simulation results with CMS and ADCIRC differed substantially, with ADCIRC showing much lower current values using standard parameter values. Variable parameters in the ADCIRC finite element model are numerous. In order to avoid equifinality problems, the bottom friction coefficient, C_f, was the only parameter considered modifying to make simulation results with the two models more similar. By altering the bottom friction coefficient it was possible to calibrate the ADCIRC model so that it more closely matches the inlet current results from CMS. Results show that current velocities are approximately linearly dependent on C_f.

The principal weakness of the modelling performed in the present study is the lack of measured inlet currents and water surface elevation data, which should be used for model calibration and validation. The only remaining option for this investigation was to cross-calibrate the models with respect to the most significant parameter governing the current speed, that is, the friction coefficient C_f, based on the assumption that the CMS model is more accurate in determining the hydrodynamics around the inlets. Furthermore, the record consistency and timing of available input data (tide/wind/wave) was unsatisfactory. Observed tidal data was replaced with records from tidal prediction software. Waves were completely omitted from all simulations, but their significance for the water exchange and mixing in the lagoon should be limited.

To improve the modelling, it would have been advantageous to have more recent data on the inlet and lagoon bathymetry. Long-term tidal effects were noted in the results, which extend further than the simulation run time. Examination of available wind data shows that the dominant wind speed and direction alter with the season. In order to identify the long-term tidal constituent and to fully evaluate the wind effect on internal circulation and exchange rate, longer simulation duration is necessary. To increase accuracy of the model parameterization, hence the model simulation results, the single most important improvement is to acquire calibration and validation data.

Despite the numerous model weaknesses some important conclusions and recommendations can be drawn: forcing as a result of tidal motion governs the exchange rate and to maintain a sufficient circulation and renewal time the model results consistently show that the east inlet is responsible for a larger portion of water

being exchanged with the Mediterranean Sea, regardless of selected scenario. The undisputed governing force of the internal circulation is the wind, whereas in proximity of the inlets, the tidal motion is more important.

Even though calibration based on observed data was not possible, the alternative cross-calibration between the models provided the results with some strength. The models used in this study have been employed in a number of similar studies giving confidence to the results obtained here, although no site-specific calibration was possible.

8 References

Abdallah, A M, El-Gindy, A A and Debes, E A. 2006. Sea level changes at Rosetta promontory, Egypt. *Egyptian Journal of Aquatic Research.* 2006, Vol. 32, 1, pp. 34-47.

Buttolph, A M, Reed, C W, Kraus, N C, Ono, N, Larson, M, Camenen, B, Hanson, H, Wamsley, T and Zundel, A K. 2006. *Two-Dimensional Depth-Averaged Circulation Model CMS-M2D: Version 3.0, Report 2, Sediment Transport and Morphology Change.* Vicksburg, MS : Coastal and Hydraulics Laboratory, U.S. Army Engineer Research and Development Center, 2006.

El-Bana, M, Bogaert, J, Hecke, P V and Khedr, A H. 2002. Vegetation Composition of a Threatened Hypersaline Lake (Lake Bardawil) North Sinai. *Plant Ecology.* 2002, pp. 163: 63-75.

Emanuelsson, D. and Mirchi, A. 2007. *Impact of coastal erosion and sedimentation along the northern Sinai coast.* s.l. : Lund University, 2007.

Fanos, A., Khafayg, A., Anwar, M. and Naffaa, M. 1994. Assessment and recommendations for the enhancement of the Bardawil Lagoon outlets. *Coastal Dynamics.* 1994, pp. 189-204.

Ferrarin, C and Umgiesser, G. 2005. Hydrodynamic modeling of a coastal lagoon: The Cabras lagoon in sardinia, Italy. *Ecological Modelling.* 17 May 2005, 188, pp. 340-357.

Frihy, O E and Lotfy, M F. 1997. Shoreline Changes and Beach-sand Sorting along the Northern Sinai Coast of Egypt. *Geo-Marine Letters.* 1997, pp. 17: 140-146.

Frihy, O E, Badr, A A, El Sayed, W R and Selim, M A. 2002. Environmental Impacts of El Arish Power Plant on the Mediterranean Coast of Sinai, Egypt. *Environmental Geology.* 2002, pp. 42: 604-611.

Inman, D L and Jenkins, S A. 1984. The Nile Littoral Cell and Man's Inpact on the Coastal Zone of the South Eastern Mediterranean. *Coastal Engineering.* 1984, pp. Chapter 109: 1600-1617.

Inman, D L. 2005. Littoral Cells. [book auth.] M L Schwartz. *Encyclopedia of Coastal Science.* 2005, pp. 594-599.

Kjerfve, B, Schettini, C A F, Knoppers, B, Lessa, G and Ferreira, H O. 1996. Hydrology and Salt Balance in a Large, Hypersaline Coastal Lagoon: Lagoa de Araruama, Brazil. *Estuarine, Coastal and Shelf Science.* 1996, Vol. 42, pp. 701-725.

Klein, M. 1986. Morphological changes of the artificial inlets of the Bardawil Lagoon. *Journal of Estuarine, Coastal and Shelf Science.* 1986, Vol. 22, pp. 487-493.

Levy, Y. 1974. Sedimenatry reflection of depositional environment in the Bardawil Lagoon, Northern Sinai. *Journal of Sedimentary Petrology.* March 1974, Vol. 44, 1, pp. 219-227.

Levy, Y. 1977. Description and mode of formation of the supratidal evaporite facies in the northern Sinai coastal plain. *Journal of Sedimentary Petrology.* 1977, Vol. 47, 1, pp. 463-474.

Miller, M J, Pietrafesa, J L and Smith, N P. 1990. *Principles of hydraulic management of coastal lagoons for aquaculture and fisheries.* No. 314. Rome : FAO Fisheries Technical Paper, 1990. p. 88.

Oertel, G F. 2005. Coastal Lakes and Lagoons. [book auth.] M L Schwartz. *Encyclopedia of Coastal Science.* 2005, pp. 263-265.

Pritchard, D W. 1960. Salt Balance and Exchange Rate for Chincoteague Bay. *Chesapeake Science.* 1960, Vol. 1, pp. 48-57.

US Army Corps of Engineers, B. 1984. *Shore Protection Manual.* Washington : US Army Corps, 1984.

Vinja, J. 1970. *Coastal inlets of Bardawil lagoon, Feasibility Study.* s.l. : Delft Hydraulics, 1970.

Unpublished works cited

Coastal Research Institute, a. 2008. *Hydrological study for Al-Zaranik wetland.* Alexandria : Unpublished, 2008.

Coastal Research Institute, b. 1971-1999. *Technical Reports.* Alexandria : Unpublished, 1971-1999.

Inman, D. 1970. *Background information on Bardawil lagoon.* s.l. : Israel Army Comannd in the Gaza Strip, 1970.

Inman, D.L. and Harris, R.W. 1970. *Preliminary report on the inlets of Bardawil lagoon.* s.l. : Unpublished, 1970.

Web references

adcirc.org. 2008. Introduction to ADCIRC. *ADCIRC.* [Online] 06 02 2008. [Cited: 06 07 2008.] www.adcirc.org.

ADG. 2006. Hurricane Katrina hindcasts. *ADCIRC Development Group.* [Online] 21 February 2006. [Cited: 10 September 2008.] http://www.nd.edu/~adcirc/katrina.htm.

FHWA. 2008. HEC 25 - Tidal Hydrology, Hydraulics, and Scour at Bridges. *U.S. Department of Transportation.* [Online] 14 June 2008. [Cited: 10 September 2008.] http://www.fhwa.dot.gov/engineering/hydraulics/hydrology/hec25appe.cfm.

Flater, Dave. 2007. WXTide32. [Online] 25 February 2007. [Cited: 15 August 2008.] http://www.wxtide32.com/index.html

Google, Earth. 2007. Google Earth. [Online] 13 November 2007. [Cited: 6 February 2008.] http://www.earth.google.com.

Lagoon. 2008. *Encyclopedia Britannica.* [Online] 2008. [Cited: April 15, 2008.] http://www.britannica.com/eb/article-9046833.

Luettich, R and Westrink, J. 2004. *Formulation and numerical implementation of the 2D/3D ADCIRC finite element model version 44.xx.* University of North Carolina at Chapel Hill & University of Notre Dame. Morehead City, NC : http://www.adcirc.org, 2004.

NOAA/NGDC&WDC for MGG Boulder. 2008. International Bathymetric Chart of the Mediterranean (IBCM). *NGDC.* [Online] 3 June 2008. [Cited: 28 May 2008.] http://www.ngdc.noaa.gov/mgg/ibcm/seismicity/.

ramsar.org. 1991. Ramsar. *Report No. 26: Preliminary mission to Egypt.* [Online] 04 10 1991. [Cited: 09 07 2008.] http://www.ramsar.org/ram/ram_rpt_26e.htm.

Troussellier, Marc. 2007. Coastal Lagoon. *The Encyclopedia of Earth.* [Online] August 13, 2007. [Cited: April 4, 2008.] http://www.eoearth.org/article/Coastal_lagoon.

US Army Corps of Engineers, A. 2007. Engineer Research and Development Center. Coastal Modeling System (CMS). [Online] September 2007. [Cited: February 6, 2008.] www.erdc.usace.army.mil.

Interview

Dr. Madhat, Abdel Mohsen Ali Mohamed. 2008. Information about Bardawil Lagoon. *Coastal Research Institute.* Alexandria, 28 July 2008.

9 Appendix

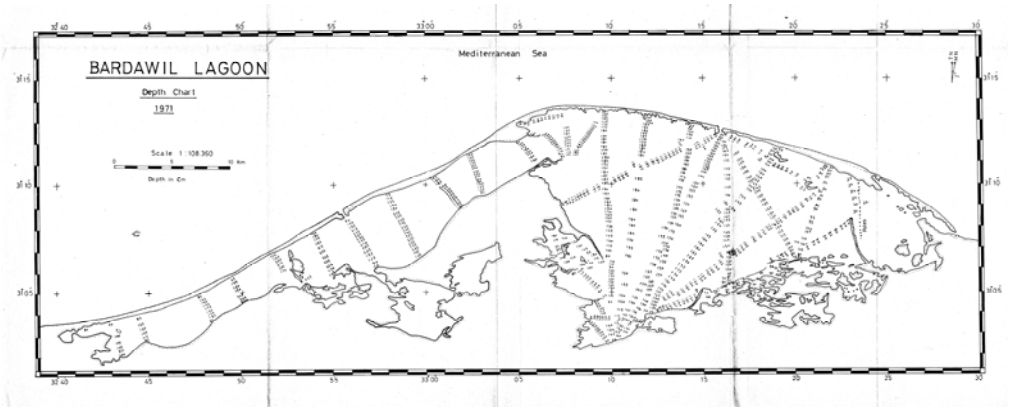

Figure 65: Bathymetry transects of Bardawil lagoon (Coastal Research Institute, 1971-1999)